Journal of Theoretical Biology 562 (2023) 111415

Contents lists available at ScienceDirect

Journal of Theoretical Biology

journal homepage: www.elsevier.com/locate/yjtbi

Long-distance hormone transport via the phloem

Heather L. Collis [a], Markus R. Owen [a], Leah R. Band [a,b,*]

[a] Centre for Mathematical Medicine and Biology, School of Mathematical Sciences, University of Nottingham, Nottingham, NG7 2RD, UK
[b] Division of Plant and Crop Sciences, School of Biosciences, University of Nottingham, Sutton Bonington Campus, Loughborough, LE12 5RD, UK

ARTICLE INFO

Dataset link: https://gitlab.com/leahband/phloem_hormone_model

Keywords:
Phloem transport
Plant hormones
Sugar transport
Münch pressure flow
Low Münch number
Arabidopsis

ABSTRACT

Several key plant hormones are synthesised in the shoot and are advected within the phloem to the root tip. In the root tip, these hormones regulate growth and developmental processes, and responses to environmental cues. However, we lack understanding of how environmental factors and biological parameters affect the delivery of hormones to the root tip. In this study, we build on existing models of phloem flow to develop a mathematical model of sugar transport alongside the transport of a generic hormone. We derive the equations for osmotically driven flow in a long, thin pipe with spatially varying membrane properties to capture the phloem loading and unloading zones. Motivated by experimental findings, we formulate solute membrane transport in terms of passive and active components, and incorporate solute unloading via bulk flow (i.e. advection with the water efflux) by including the Staverman reflection coefficient. We use the model to investigate the coupling between the sugar and hormone dynamics. The model predicts that environmental cues that lead to an increase in active sugar loading, an increase in bulk flow sugar unloading or a decrease in the relative root sugar concentration result in an increase in phloem transport velocity. Furthermore, the model reveals that such increases in phloem transport velocity result in an increase in hormone delivery to the root tip for passively loaded hormones.

1. Introduction

The phloem forms part of a plant's vascular system and is responsible for the long-distance transport of sugars, proteins, and hormones from the shoot to the root (Taiz and Zeiger, 2010). Many studies have shown that shoot-derived hormones are transported long distances within the phloem to regulate developmental processes in the root (Lacombe and Achard, 2016; Baker, 2000). The transport of the gibberellin (GA) precursor GA_{12} through the Arabidopsis phloem acts as a long-distance signal mediating growth responses (Regnault et al., 2015). Translocation of cytokinins from shoot to root via the phloem is important for nitrogen acquisition (Kiba et al., 2011), the regulation of root nodulation (Sasaki et al., 2014), and maintenance of vascular patterning in the root (Bishopp et al., 2011). Lateral root development has been shown to depend on long-distance transport of both auxin (Bhalerao et al., 2002; Chhun et al., 2007) and ABA (Zhang et al., 2021).

Although it is well established that hormones are advected through the phloem (Lacombe and Achard, 2016), as far as we are aware no previous mathematical models have considered this directly and investigated how parameters affect hormone delivery from the shoot to the root tip. Instead, existing plant-hormone models focus on hormone dynamics within a specific organ or tissue, for example, modelling auxin dynamics in the root tip. These root-tip models typically assume there is a fixed auxin concentration at the boundary between the modelled root-tip tissue and the region of long-distance transport (Grieneisen et al., 2007; Band et al., 2012; van den Berg et al., 2016; Mellor et al., 2020). However, the processes that regulate the auxin dynamics at this boundary have not been studied directly.

Existing mathematical models of phloem transport focus on the movement of sugars through the phloem via the pressure flow hypothesis (Minchin et al., 1993; Bidel et al., 2000; Thompson and Holbrook, 2003a; Jensen et al., 2011, 2012; Payvandi et al., 2014; Jensen et al., 2016; van den Herik et al., 2021; Nakad et al., 2021) initially proposed by Münch (1926); this describes how phloem sap movement is generated by osmotic pressure differences caused by a gradient in sugar concentration between source and sink tissues (Jensen et al., 2016). Sugar is loaded into the phloem at the shoot, reducing the phloem sap osmotic potential and causing an influx of water, whereas sugar unloading in the root increases the phloem osmotic potential causing water efflux. The resulting gradient in hydrostatic pressure drives phloem

* Corresponding author at: Division of Plant and Crop Sciences, School of Biosciences, University of Nottingham, Sutton Bonington Campus, Loughborough, LE12 5RD, UK.
E-mail address: leah.band@nottingham.ac.uk (L.R. Band).

https://doi.org/10.1016/j.jtbi.2023.111415
Received 21 June 2022; Received in revised form 20 December 2022; Accepted 10 January 2023
Available online 18 January 2023

water flow that advects the sugar and other solutes (Payvandi et al., 2014). Key developments from previous models include non-steady-state dynamics (Thompson and Holbrook, 2003a), the development of analytical solutions in high and low Münch number limits (Jensen et al., 2012), and investigating the importance of diffusion in boundary layers at high Münch number (Payvandi et al., 2014). Many of these models have focused on larger plant species such as barley (Minchin et al., 1993), peach (Bidel et al., 2000), and black locust (Payvandi et al., 2014) which have a Münch number greater than 1.

In this study, we expand upon the phloem transport models in the literature to include the transport of a generic hormone (though we note that the model presented is also applicable to the transport of any small passively advected molecules in the phloem). Our model also includes adaptations that allow us to capture more realistic loading and unloading mechanisms. This formulation enables us to represent specific physical processes such as passive diffusion through plasmodesmata and active transport via known membrane proteins. Motivated by experimental findings (Ross-Elliott et al., 2017; Bret-Harte and Silk, 1994), we also incorporate loading and unloading via bulk flow, by introducing the Staverman reflection coefficient (Staverman, 1951) which allows for solutes to leak across the membrane in the direction of water flow. In the results section, we focus on model scenarios with low Münch number, representative of smaller plants such as *Arabidopsis thaliana*, for which bulk flow has been shown to be the dominant form of phloem unloading (Ross-Elliott et al., 2017).

2. Model derivation

2.1. Model description

In order to formulate the mathematical model, we consider the phloem to be a long, thin, narrow pipe through which water and solutes are transported. The phloem is split into three zones: the loading zone ($x \in [0, x_1]$); translocation zone ($x \in [x_1, x_2]$); and unloading zone ($x \in [x_2, x_3]$), where x denotes the distance along the phloem. The radius of the phloem tube is a and the length of the translocation zone is given by $L = x_2 - x_1$, (where $a \ll L$). Water can flow into and out of the phloem tube along the entire length of the pipe. However, solutes may only enter/leave the phloem in the loading/unloading zone respectively. Water is considered to be transferred to/from the xylem, whereas solutes are considered to be transferred to/from sink/source tissues. The phloem tube walls are comprised of membranes with permeability properties that depend on the distance along the phloem tube. A schematic of the modelling structure is given in Fig. 1.

In reality, the vascular system of a seedling is more complex than shown in Fig. 1, and varies quite dramatically along the length of a seedling (Fig. 2, De Rybel et al., 2016). Throughout the seedling, the two key vascular tissues, xylem and phloem, are present and separated by a region of procambial cells (Fig. 2). As such, any transfer of water from xylem to phloem must pass through the intervening tissue. In its simplest form, the structure of the vascular system of a plant can be represented by Fig. 1A which for mathematical simplicity is described by a set of concentric annuli as shown in Fig. 1B.

We consider a steady-state formulation. We model the phloem sap (water with dissolved solutes) as an incompressible Newtonian fluid, with velocity in the longitudinal and radial directions given by $v_x(r,x)$ and $v_r(r,x)$ respectively, hydrostatic pressure $p_p = p_p(r,x)$, and osmotic potential $\pi_p(r,x)$ where x denotes the distance along the phloem tube and r the radial position within the phloem. The concentration of solute in the phloem is given by $c_p(r,x)$. The model solutions depend on the concentration of solute in the xylem $c_x(x)$ and in the external source/sink tissues $c_{ext}(x)$, and the hydrostatic pressure and osmotic potential in the xylem, $p_x(x)$ and $\pi_x(x)$ respectively.

Throughout the model derivation, we use nondimensionalised variables defined by,

$$x = LX, \qquad r = aR, \qquad Re = \frac{\rho U L}{\eta},$$
$$v_x = UV_x \qquad v_r = \varepsilon U V_r, \qquad Pe = \frac{UL}{D},$$
$$(p_p, p_x) = \frac{\eta L U}{a^2}(P, P_x), \quad (\pi_p, \pi_x) = P^*(\Pi, \Pi_x) \quad (c_p, c_x, c_{ext}) = C^*(C, C_x, C_{ext}),$$

where U is a characteristic flow speed of the phloem sap in the x-direction, η is the viscosity of the phloem sap, ρ is the phloem sap density, D is the diffusivity coefficient of water, C^* is the solute concentration in the external source tissue at $X = 0$, and P^* is the scale parameter for osmotic pressure.

Water flow between the xylem and phloem is driven by differences in the hydrostatic and osmotic pressure (Jensen et al., 2011). Moving straight to the non-dimensionalised equations (using the nondimensionalised variables above), the velocity of the water moving from the xylem into the phloem, $\mathscr{V}(X)$, at the phloem membrane boundary is

$$\mathscr{V}(X) = \frac{1}{2}\left(\frac{\text{Mü}}{8}(P_x(X) - P(1,X)) - \frac{2L_p P^*}{\varepsilon U}\sigma(\Pi_x(X) - \Pi(1,X))\right), \tag{1}$$

where L_p is the membrane water permeability, $\text{Mü} = 16\eta L_p L^2/a^3$ is the Münch number which represents the ratio between radial and axial conductivity (Thompson and Holbrook, 2003b; Jensen et al., 2009), and $\sigma = \sigma(X)$ is the Staverman reflection coefficient (Staverman, 1951; Truskey et al., 2010b). The Staverman reflection coefficient varies between zero and one, where $\sigma = 1$ represents a perfectly semi-permeable membrane, permeable only to water, and $\sigma = 0$ represents a membrane that is permeable to both water and solute equally. Values between zero and one represent membranes that are semi-permeable but with some leakage of solute along with the water (Truskey et al., 2010b). Applying the van't Hoff equation (Truskey et al., 2010b), the osmotic potentials can be related to the solute concentrations via,

$$P^*\Pi(R,X) = RTC^*C(R,X), \qquad P^*\Pi_x(X) = RTC^*C_x(X), \tag{2}$$

where R is the ideal gas constant and T is the absolute temperature.

We define the flux of solute from the phloem to the surrounding tissues, J_s, by

$$J_s = J_v(1-\sigma)\bar{C} + \beta(C - C_{ext}) - \gamma C + \lambda C_{ext}, \tag{3a}$$
$$\bar{C} = \frac{(C_{ext} + C)}{2}, \tag{3b}$$

where J_v is the fluid velocity across the membrane (in this case $J_v = -\mathscr{V}(X)$), $\bar{C}$ is the average concentration inside the membrane, β is the rate of solute diffusion across the membrane (Truskey et al., 2010b), γ is the rate of active loading, and λ is the rate of active unloading. The first term on the right-hand-side of Eq. (3a) represents solute being dragged across the phloem membrane with the flow of water, whereas the second term represents passive diffusion through the phloem-tissue membrane. These two terms form the solute flux equation of Kedem and Katchalsky (1958). The final two terms in (3a) represent active transport of solute into and out of the phloem. The equation for solute flux, (3a), varies from previous phloem models as they assumed the membrane of the phloem was perfectly semi-permeable ($\sigma = 1$) (Jensen et al., 2012; Payvandi et al., 2014; Jensen et al., 2016). Furthermore, by formulating the solute flux, (3a), in terms of passive and active components that depend on the external concentrations, the model parameters relate directly to biological processes that can be perturbed experimentally and can vary in response to environmental conditions.

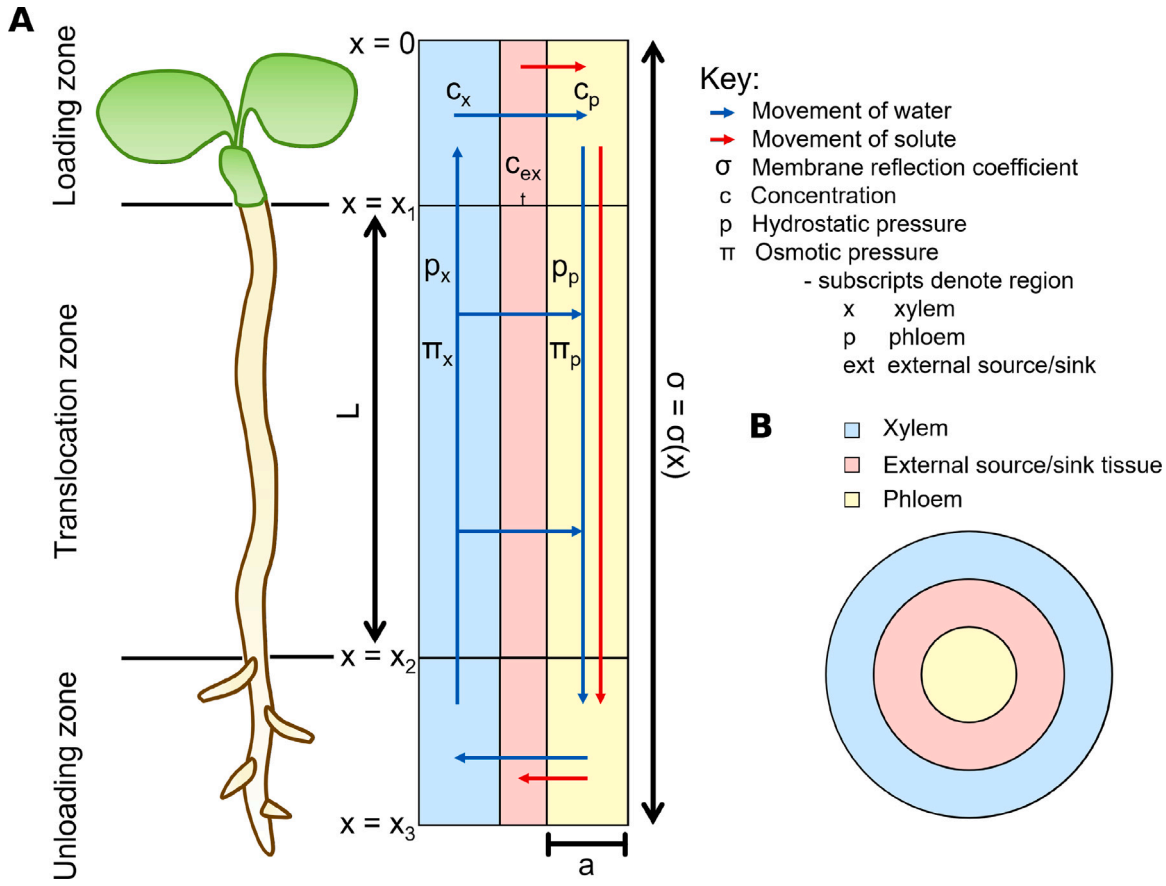

Fig. 1. **(A)** Schematic showing the modelling structure of the phloem and surrounding tissues. The phloem is considered a long thin pipe split into three zones (loading, translocation, unloading). Water is considered to be transferred directly from xylem to phloem (and the xylem contains no solute), whereas the solute is transferred to/from an external tissue sink/source. **(B)** Mathematically this structure is described by a set of concentric annuli.

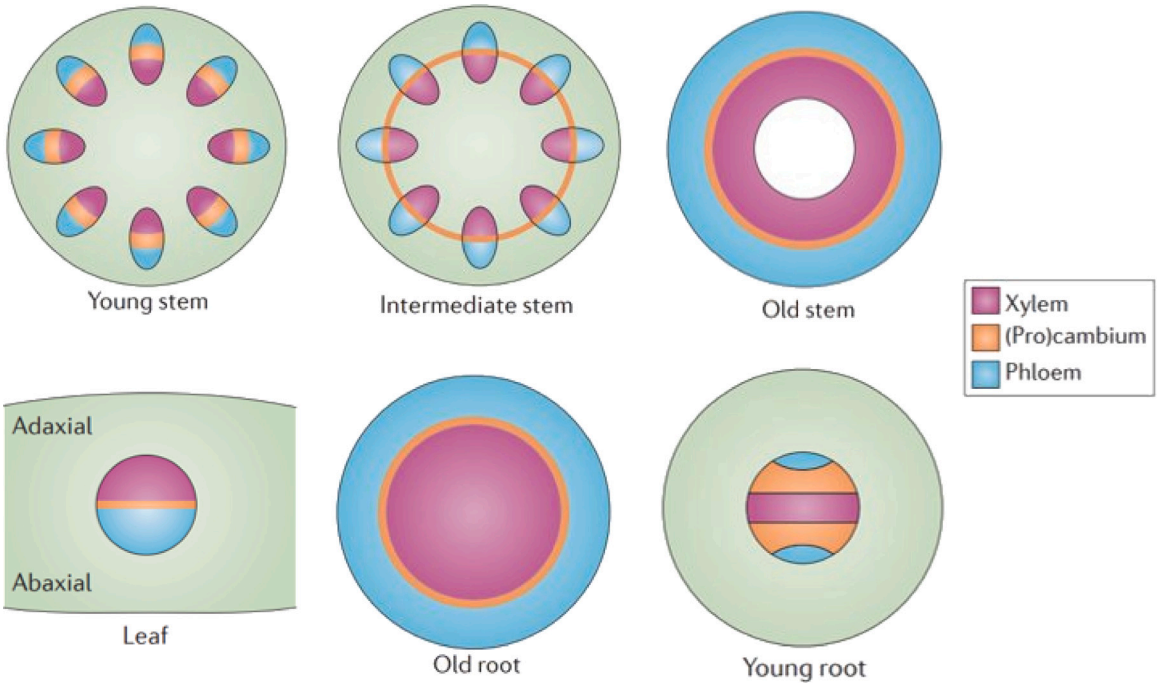

Fig. 2. Schematic of plant vascular structure throughout a plant .
Source: Adapted from De Rybel et al. (2016).

2.2. Governing equations

Given $\varepsilon = a/L \ll 1$ (and noting we take $\varepsilon^2 Re \ll 1$), the fluid velocity is governed by the leading-order lubrication equations (Truskey et al., 2010a),

$$\frac{1}{R}\frac{\partial}{\partial R}(RV_{r,0}) + \frac{\partial V_{x,0}}{\partial X} = 0 \tag{4a}$$

$$\frac{\partial P_0}{\partial X} = \frac{1}{R}\frac{\partial}{\partial R}\left(R\frac{\partial V_{x,0}}{\partial R}\right), \tag{4b}$$

$$\frac{\partial P_0}{\partial R} = 0, \tag{4c}$$

with boundary conditions,

$$V_{x,0}(1,X) = 0, \quad \text{(no slip condition at membrane boundary)} \tag{5a}$$

$$\left.\frac{\partial V_{x,0}}{\partial R}\right|_{(0,X)} = 0, \quad \text{(symmetry about the centre-line)} \tag{5b}$$

$$V_{x,0}(R,0) = 0, \quad \text{(no axial flux at ends of phloem tube)} \tag{5c}$$

$$V_{x,0}(R,X_3) = 0, \quad \text{(no axial flux at ends of phloem tube)} \tag{5d}$$

$$V_{r,0}(0,X) = 0, \quad \text{(symmetry about the centre-line)} \tag{5e}$$

$$V_{r,0}(1,X) = -\mathscr{V}(X), \quad \text{(continuity of velocity at the membrane)} \tag{5f}$$

where the subscript 0 denotes the leading-order components as $\varepsilon \to 0$.

The concentration dynamics are described by the steady-state advection–diffusion equation,

$$\varepsilon^2 Pe\left(\frac{\partial}{\partial X}(CV_x) + \frac{1}{R}\frac{\partial}{\partial R}(RCV_r)\right) = \frac{1}{R}\frac{\partial}{\partial R}\left(R\frac{\partial C}{\partial R}\right) + \varepsilon^2\frac{\partial^2 C}{\partial X^2}, \tag{6}$$

with the boundary conditions given by equating the outward normal solute flux at the boundary of the phloem to the equation for solute flux, (3a), and no axial flux at the end points of the phloem,

$$\left.\frac{\partial C}{\partial R}\right|_{(1,X)} = \varepsilon^2 Pe\big[C(1,X)V_r(1,X) - (1-\sigma)\bar{C}V_r(1,X) + \beta(C_{ext}(X) - C(1,X)) + \gamma C_{ext}(X) - \lambda C(1,X)\big], \tag{7a}$$

$$\left.\frac{\partial C}{\partial X}\right|_{(R,0)} = 0, \tag{7b}$$

$$\left.\frac{\partial C}{\partial X}\right|_{(R,X_3)} = 0. \tag{7c}$$

Substituting the expansion $C = C_0 + \varepsilon^2 C_1 + \cdots$ into Eqs. (6) and (7), yields at leading order,

$$\frac{1}{R}\frac{\partial}{\partial R}\left(R\frac{\partial C_0}{\partial R}\right) = 0, \tag{8a}$$

$$\left.\frac{\partial C_0}{\partial X}\right|_{(R,0)} = 0, \tag{8b}$$

$$\left.\frac{\partial C_0}{\partial X}\right|_{(R,X_3)} = 0. \tag{8c}$$

We note that in specifying (8a), we assume that $\epsilon^2 Pe \ll 1$ which results in radial diffusion dominating so that the leading-order concentration depends only on X.

At $O(\varepsilon^2)$, Eqs. (6) and (7a) yield,

$$Pe\left(V_{x,0}\frac{\partial C_0}{\partial X} + \frac{C_0}{R}\frac{\partial}{\partial R}(RV_{r,0}) + C_0\frac{\partial V_{x,0}}{\partial X}\right) = \frac{\partial^2 C_0}{\partial X^2} + \frac{1}{R}\frac{\partial}{\partial R}\left(R\frac{\partial C_1}{\partial R}\right), \tag{9a}$$

$$\left.\frac{\partial C_1}{\partial R}\right|_{(1,X)} = Pe\big[C_0(X)V_{r,0}(1,X) - (1-\sigma)\bar{C}V_{r,0}(1,X) + \beta(C_{ext}(X) - C_0(X)) + \gamma C_{ext}(X) - \lambda C_0(X)\big]. \tag{9b}$$

To close the system, it remains to specify $\mathscr{V}$ at leading order. Applying leading-order expansions to Eqs. (1) and (2), we obtain the leading-order velocity across the membrane,

$$\mathscr{V}_0(X) = \frac{1}{2}\left(\frac{\text{Mü}}{8}(P_x(X) - P_0(X)) - \sigma(C_x(X) - C_0(X))\right), \tag{10}$$

where we have equated the characteristic radial flow speed to that driven by osmotic potential via $\varepsilon U = 2L_p RTC^*$ (Jensen et al., 2016).

2.2.1. Averaging in the radial direction

Following the work of Jensen et al. (2012), Payvandi et al. (2014), Jensen et al. (2016), we can reduce the system complexity by integrating the governing Eqs. (4) and (9a) with respect to R.

Given the leading-order pressure is a function of X only, (4c), we integrate (4a), (4b) with respect to R, and apply boundary conditions (5e), (5b), (5a), which gives

$$V_{x,0}(R,X) = \frac{(R^2-1)}{4}\frac{\partial P_0}{\partial X}, \tag{11a}$$

$$V_{r,0}(R,X) = \frac{\partial^2 P_0}{\partial X^2}\frac{(2R - R^3)}{16}. \tag{11b}$$

Evaluating (11b) at $R = 1$, (5f) then gives

$$\frac{\partial^2 P_0}{\partial X^2} = 16\mathscr{V}_0(X). \tag{12}$$

Integrating (9a) with respect to R and substituting (11a) and (11b), we obtain,

$$Pe\left[\left(\frac{\partial C_0}{\partial X}\frac{\partial P_0}{\partial X} + C_0\frac{\partial^2 P_0}{\partial X^2}\right)\left(\frac{R^4 - 2R^2}{16}\right) + RC_0V_{r,0}\right] = \frac{R^2}{2}\frac{\partial^2 C_0}{\partial X^2} + R\frac{\partial C_1}{\partial R}, \tag{13}$$

(where the constant of integration must be zero for consistency at $R = 0$). Evaluating at $R = 1$ and applying boundary conditions (5f) and (9b) yields,

$$-\frac{1}{16}\left(\frac{\partial C_0}{\partial X}\frac{\partial P_0}{\partial X} + C_0\frac{\partial^2 P_0}{\partial X^2}\right) = (1-\sigma)\bar{C}\mathscr{V}_0(X) + \beta(C_{ext}(X) - C_0(X)) + \gamma C_{ext}(X) - \lambda C_0(X) + \frac{1}{2Pe}\frac{\partial^2 C_0}{\partial X^2}. \tag{14}$$

To reduce to a one-dimensional system, we write the governing equations in terms of the average axial flow speed, given by $\bar{U}(X) = Q(X)/\pi$ where $Q(X)$ is the volumetric flow rate:

$$\bar{U}(X) = \frac{Q(X)}{\pi} = \int_0^1 2RV_{x,0}(R,X)\,dR = -\frac{1}{8}\frac{\partial P_0}{\partial X}. \tag{15}$$

Substituting for $\partial P_0/\partial X$, (15), and $\mathscr{V}_0$, (10), into Eqs. (12) and (14), we obtain a closed system of equations for $\bar{U}(X), C_0(X)$, and $P_0(X)$:

$$\frac{\partial \bar{U}}{\partial X} = \sigma(C_0 - C_x) - \frac{\text{Mü}}{8}(P_0 - P_x), \tag{16a}$$

$$\frac{\partial \bar{U}C_0}{\partial X} = \frac{1}{Pe}\frac{\partial^2 C_0}{\partial X^2} + (1-\sigma)\bar{C}\left(\sigma\left(C_0 - C_x\right) - \frac{\text{Mü}}{8}\left(P_0 - P_x\right)\right) + 2\beta(C_{ext} - C_0) + 2\gamma C_{ext} - 2\lambda C_0 \tag{16b}$$

$$\frac{\partial P_0}{\partial X} = -8\bar{U}, \tag{16c}$$

where $\bar{C}$ is given by Eq. (3b) and the boundary conditions (reduced to one-dimension from (5c), (5d)) are given by,

$$\bar{U}(0) = 0, \quad \bar{U}(X_3) = 0, \tag{17a}$$

$$\left.\frac{\partial C_0}{\partial X}\right|_{(0)} = 0, \quad \left.\frac{\partial C_0}{\partial X}\right|_{(X_3)} = 0. \tag{17b}$$

We note that by differentiating Eq. (16a) and setting $\sigma = 1$, we would obtain Münch flow equations similar to those in previous studies (Thompson and Holbrook, 2003a; Jensen et al., 2012; Payvandi et al., 2014; Jensen et al., 2016).

2.3. Modelling hormone transport in the phloem

Eqs. (16) describe the leading-order phloem transport for a single solute (sugar). We now extend these equations (dropping the subscript 0 for simplicity) to incorporate a hormone (or other passively advected solute). We use the notation C_s and C_a to represent the leading-order

concentration of sugar and hormone respectively. Hormone molecules are tiny compared to sugar molecules, and so it is appropriate to assume that the hormone concentration does not contribute significantly to the osmotic pressure gradient. Due to the Péclet number for sugar and a range of plant hormones being large (see Appendix A), we assume, in line with models in the literature (Jensen et al., 2012, 2016), that axial diffusion is negligible and hence the equations governing the transport of hormone and sugar via the phloem are given by,

$$\frac{\partial \bar{U}}{\partial X} = \sigma(C_s(X) - C_{x,s}(X)) - \frac{\text{Mü}}{8}(P(X) - P_x(X)), \tag{18a}$$

$$\frac{\partial \bar{U} C_s}{\partial X} = (1-\sigma_s)\bar{C}_s\left(\sigma_s(C_s(X) - C_{x,s}(X)) - \frac{\text{Mü}}{8}(P(X) - P_x(X))\right) + 2\beta_s(C_{ext,s}(X) - C_s(X)) + 2\gamma_s C_{ext,s}(X) - 2\lambda_s C_s(X), \tag{18b}$$

$$\frac{\partial \bar{U} C_a}{\partial X} = (1-\sigma_a)\bar{C}_a\left(\sigma_s(C_s(X) - C_{x,s}(X)) - \frac{\text{Mü}}{8}(P(X) - P_x(X))\right) + 2\beta_a(C_{ext,a}(X) - C_a(X)) + 2\gamma_a C_{ext,a}(X) - 2\lambda_a C_a(X), \tag{18c}$$

$$\frac{\partial P}{\partial X} = -8\bar{U}(X), \tag{18d}$$

where,

$$\bar{C}_s = \frac{C_s + C_{ext,s}}{2}, \qquad \bar{C}_a = \frac{C_a + C_{ext,a}}{2}, \tag{19}$$

and the boundary conditions are given by

$$\bar{U}(0) = 0, \qquad \bar{U}(X_3) = 0. \tag{20}$$

2.4. Representing the loading and unloading zones

To represent the loading and unloading zones, we define the spatially dependent coefficients of solute transport and external solute concentrations as step functions between zones (loading=1, translocation=2, unloading=3). In the functions below X_1, X_2, X_3 represent the end points of the loading, translocation, and unloading zone respectively with $X_1 = 0.2, X_2 = 1.2$, and $X_3 = 1.4$ for consistency with loading and unloading zones prescribed in Jensen et al. (2012):

$$\mathscr{B}_k(X) = \begin{cases} \mathscr{B}_{k,1}, & 0 \le X \le X_1; \\ \mathscr{B}_{k,2}, & X_1 < X < X_2; \\ \mathscr{B}_{k,3}, & X_2 \le X \le X_3, \end{cases} \tag{21}$$

For notational convenience, here, $\mathscr{B}_k$ is used represent a general parameter where $\mathscr{B} \in \{\sigma, \beta, \gamma, \lambda, C_{ext}\}$ and the subscript $k \in \{s, a\}$ denotes sugar and hormone respectively.

Model solutions enable us to calculate the total flux of sugar and hormone into the loading zone and out of the unloading zone by integrating Eqs. (18b) and (18c) with respect to X across the length of the loading and unloading zone respectively,

$$F_s(l_1, l_2) = \int_{l_1}^{l_2} \frac{\partial U C_s}{\partial X} dX = \int_{l_1}^{l_2} \left[(1-\sigma_s)\bar{C}_s\left(\sigma_s(C_s(X) - C_{x,s}(X)) - \frac{\text{Mü}}{8}(P(X) - P_x(X))\right) + 2\beta_s(C_{ext,s}(X) - C_s(X)) + 2\gamma_s C_{ext,s}(X) - 2\lambda_s C_s(X)\right] dX, \tag{22a}$$

$$F_a(l_1, l_2) = \int_{l_1}^{l_2} \frac{\partial U C_a}{\partial X} dX = \int_{l_1}^{l_2} \left[(1-\sigma_a)\bar{C}_s\left(\sigma_s(C_s(X) - C_{x,s}(X)) - \frac{\text{Mü}}{8}(P(X) - P_x(X))\right) + 2\beta_a(C_{ext,a}(X) - C_a(X)) + 2\gamma_a C_{ext,a}(X) - 2\lambda_a C_a(X)\right] dX; \tag{22b}$$

setting $l_1 = 0$ and $l_2 = X_1$ in (22) corresponds to the loading zone, and setting $l_1 = X_2$ and $l_2 = X_3$ corresponds to the unloading zone. Eqs. (22) are defined in terms of fluxes into the phloem and so unloading results in a negative value.

Table 1
Default values for sugar parameters.

Parameter group	Default values	Parameter description
$(\sigma_{s,1}, \sigma_{s,2}, \sigma_{s,3})$	$(1, 1, 0 \le \sigma_{s,3} \le 1)$	Bulk flow
$(\beta_{s,1}, \beta_{s,2}, \beta_{s,3})$	$(0, 0, 5)$	Passive diffusion
$(\gamma_{s,1}, \gamma_{s,2}, \gamma_{s,3})$	$(0.16, 0, 0)$	Active loading
$(\lambda_{s,1}, \lambda_{s,2}, \lambda_{s,3})$	$(0, 0, 0)$	Active unloading
$(C_{ext,s,1}, C_{ext,s,2}, C_{ext,s,3})$	$(1, 0, 0.1)$	External sugar concentration

2.5. Numerical method

The system of Eqs. (18) along with boundary conditions (20) describe a boundary value problem where we have boundary conditions defined at both ends of the domain. In order to solve these equations numerically, we use a shooting method with shooting parameter $\partial \bar{U}(0)/\partial X$. A full description of the shooting method used in our model is available in Appendix B. We solve the system of governing equations numerically in `Python 3.8` using an upwind scheme (see Appendices C and D).

3. Prescribing biologically motivated loading and unloading parameters

We have derived the governing equations for phloem transport under general loading and unloading mechanisms. However, the results will focus on parameter regimes that represent phloem loading and unloading in Arabidopsis and crops, given experimental studies on long-distance hormone transport are predominantly in these species. Experiments have shown that the dominant mechanism for sugar loading in Arabidopsis and crops is active loading (see Table 2 in Jensen et al., 2013).

Experimental studies consider sugar unloading to be passive (Oparka et al., 1994; Imlau et al., 1999), and evidence from Ross-Elliott et al. (2017) and Bret-Harte and Silk (1994) supports this, with bulk flow unloading being the dominant efflux component. To incorporate bulk flow unloading, we set the Staverman reflection coefficient (Staverman, 1951) to be less than one in the unloading zone. This is in contrast to current models in the literature where passive sugar unloading is modelled as unloading via diffusion only (corresponding to a Staverman reflection coefficient of 1 throughout the phloem).

Based on the above considerations, Table 1 gives the default sugar parameters used throughout the simulations; these parameters were chosen to give equivalent sugar loading influx to parameters from Jensen et al. (2012), but are modified as we assume active sugar loading only.

As we are modelling for a general hormone, we simulate a variety of loading scenarios as the loading methods for different hormones are not well characterised. As such, for each set of sugar parameters, we model two distinct cases; where the hormone is loaded actively and where the hormone is loaded passively via diffusion. We note that it is likely that some hormones are loaded via a combination of both these mechanisms (such as auxin Tamas and Davies, 2016). Similarly to sugar, we assume the hormone is unloaded passively in order to investigate the impact of bulk flow on hormone delivery. As such, the parameter definitions and default values for hormone parameters are given in Table 2.

Given our model assumptions are predominantly based on data from Arabidopsis seedlings, we calculated the Münch number using the Arabidopsis parameters given in Table 3, which gives Mü= 0.22.

Table 2
Hormone parameters for passive and actively loaded hormone.

Parameter group	Passive hormone loading	Active hormone loading
$(\sigma_{a,1}, \sigma_{a,2}, \sigma_{a,3})$	$(1, 1, 0 \leq \sigma_{s,3} \leq 1)$	$(1, 1, 0 \leq \sigma_{s,3} \leq 1)$
$(\beta_{a,1}, \beta_{a,2}, \beta_{a,3})$	$(5, 0, 5)$	$(0, 0, 5)$
$(\gamma_{a,1}, \gamma_{a,2}, \gamma_{a,3})$	$(0, 0, 0)$	$(0.16, 0, 0)$
$(\lambda_{a,1}, \lambda_{a,2}, \lambda_{a,3})$	$(0, 0, 0)$	$(0, 0, 0,)$
$(C_{ext,a,1}, C_{ext,a,2}, C_{ext,a,3})$	$(1, 0, 0.1)$	$(1, 0, 0.1)$

Table 3
Parameter values required for calculating the Münch number for Arabidopsis. Values taken from Ross-Elliott et al. (2017), phloem tube length from Martin et al. (2002).

Parameter name	Symbol	Value
Phloem sap viscosity	η	1.7 mPas
Phloem tube length	L	30.6 mm
Cell membrane permeability	L_p	5×10^{-14} m/s/Pa
Phloem tube radius	a	1.8 μm

This value is much lower than previously modelled species such as wheat and black locust which have values Mü = 12 and Mü = 10^4 respectively (Payvandi et al., 2014). We note that Jensen et al. (2012) produce analytical solutions for phloem transport velocity and sugar concentration in the limit of small Münch number and show that these results have little variation from numerical solutions when Mü = 1 (albeit without the inclusion of the Staverman reflection coefficient). We note that these analytical solutions would be appropriate for simulations of phloem transport velocity and sugar concentration in Arabidopsis and our simulation results are qualitatively consistent with these results in the case when $\sigma_{s,3} = 1$. However, our mathematical model has been developed such that it can capture the phloem transport dynamics (including hormone concentration profiles) for any Münch number or loading/unloading parameters if desired. For completeness, in the results section below, we investigate the impact of bulk flow unloading in both a low and high Münch number regime as an example.

4. Results

4.1. The rate of delivery to the root tip does not depend on phloem transport velocity for actively loaded sugar and hormones

Before proceeding with the simulation results, we note that as the model is at steady state, the total flux into the phloem in the loading zone must equal the total flux out of the phloem in the unloading zone; both can be calculated using Eqs. (22). For the actively loaded sugar and in cases where the hormone is actively loaded, the total flux into the phloem depends only on the prescribed external concentration and active transport rate. As a result, the total loading and unloading flux is independent of the concentrations in the phloem and the unloading parameters. Thus, for purely actively loaded sugar and hormones, the steady-state rate of delivery to the root tip does not depend on the phloem transport velocity.

4.2. Bulk flow unloading increases the phloem transport velocity

One of the key extensions of this model is the inclusion of the Staverman reflection coefficient (Staverman, 1951), which allows the model to capture the effect of unloading via bulk flow, which Ross-Elliott et al. (2017) suggest to be the dominant unloading mechanism in Arabidopsis.

To investigate the impact of bulk flow unloading, we allow the Staverman reflection coefficient for sugar, $\sigma_{s,3}$, and the general hormone, $\sigma_{a,3}$, to vary simultaneously in the unloading zone. As discussed above, the total sugar flux into and out of the phloem in the loading and unloading does not depend on $\sigma_{s,3}$ (Fig. 3A). As one may expect, decreasing $\sigma_{s,3}$ allows for membrane leakage and hence there is more unloading via bulk flow. However, for the chosen model parameters (Tables 1 and 2), the model predicts that diffusive unloading of sugar always remains dominant over bulk flow unloading of sugar.

The phloem transport velocity and sugar concentration profile depend only on the Staverman reflection coefficient for sugar (Eqs. (18)a, b). Reducing the Staverman reflection coefficient for sugar increases bulk flow sugar unloading which results in a depletion of sugar in the phloem (Fig. 3E). As the total sugar efflux in the unloading zone is prescribed by the loading parameters, the sugar depletion caused by increased bulk flow unloading must be balanced by an increase in phloem transport velocity (Fig. 3D) to maintain the prescribed rate of sugar efflux (Eq. (22a)).

For an actively loaded hormone (Figs. 3C, G), the hormone concentration profile and bulk flow contribution directly mimics the results for sugar. For a hormone loaded passively (Fig. 3F), when σ_s is reduced the increase in phloem transport velocity also results in reduced hormone concentrations (although in this case the change is small and not perceptible in the loading zone). For passively loaded hormones, the increase in phloem transport velocity caused by decreasing $\sigma_{s,3}$ reduces hormone concentration in the loading zone in the phloem. This increases the concentration difference which drives passive loading across the membrane, leading to a larger loading flux, and hence, due to the steady-state assumption, a larger unloading flux of hormones in the root tip (Fig. 3B).

These model scenarios were repeated for a high Münch number as is typical for larger plant species (Mü = 12 Payvandi et al., 2014). Whilst the overall shape of the phloem transport velocity profile and sugar/hormone concentration profiles change significantly from the low Münch number scenario, the over-arching impact that increasing bulk flow unloading increases phloem transport velocity remains consistent with the low Münch number scenario (Fig. 4).

Table 4
Parameter ranges used in parameter searches performed in Figs. 5 and 6.

Parameter	Values
$\sigma_{s,3}$	(0.0, 0.2, 0.4, 0.6, 0.8, 1.0)
$\beta_{s,3}$	(0.1, 0.5, 1.0, 2.5, 5.0)
$\gamma_{s,1}$	(0.04, 0.08, 0.16)
$C_{ext,s,1}$	(0.1, 0.2, 0.4)

4.3. Bulk flow unloading can dominate over diffusive unloading when the ratio between root and shoot external sugar concentrations is increased

The simulations above showed that, for the model parameters given in Tables 1 & 2, the dominant form of sugar unloading is diffusion (Figs. 3). However, previous studies suggest that diffusive unloading of sugar alone would not be sufficient to meet the carbon demands for growth in the primary root tip of maize (Bret-Harte and Silk, 1994), and suggest that bulk flow unloading is the dominant form of sugar unloading in Arabidopsis (Ross-Elliott et al., 2017). Motivated by these studies, and the fact that the phloem loading/unloading parameters are not well characterised, we now investigate how the choice of model parameters influences the relative contributions of bulk flow and diffusive unloading.

We performed a systematic search for parameter sets that result in bulk flow unloading of sugar being dominant over diffusive unloading. Focusing on the four key sugar parameters: Staverman reflection coefficient, $\sigma_{s,3}$, rate of diffusive unloading, $\beta_{s,3}$, rate of active loading, $\gamma_{s,1}$, and the ratio between root and shoot external sugar concentrations, $C_{ext,s,3}$, we considered a discrete set of values for each parameter (see Table 4). From these parameter sets, we found multiple parameter regions that resulted in bulk flow unloading being dominant over diffusive unloading.

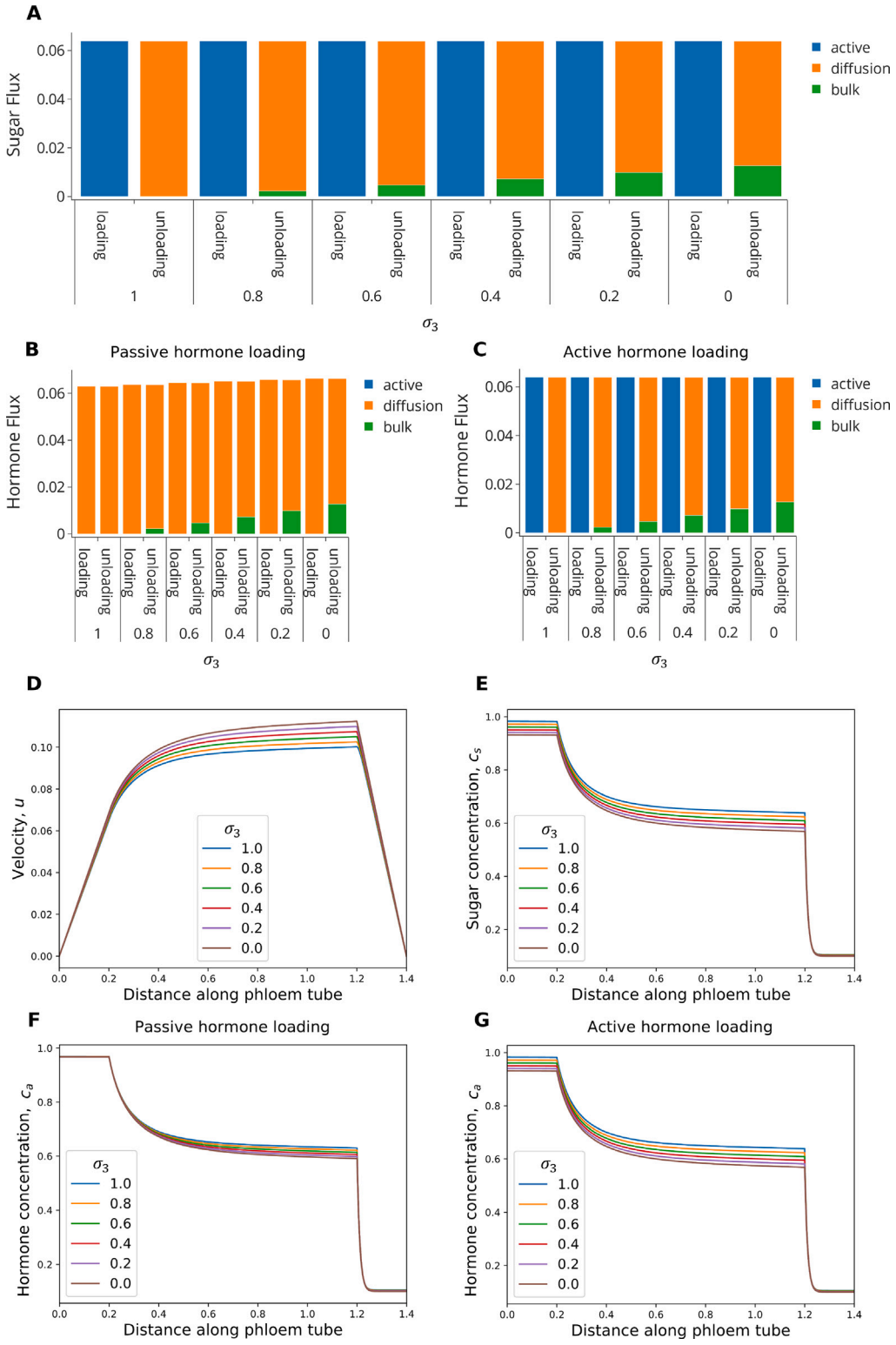

Fig. 3. Decreasing the Staverman reflection coefficient results in an increase in bulk flow unloading for sugar and hormone. Increasing the amount of bulk flow unloading increases the phloem transport velocity and decreases the concentration of sugar in the loading zone. This results in increased hormone unloading for both passively and actively loaded hormone. **(A)** Sugar flux in the loading/unloading zones; **(B)** Hormone flux in the loading/unloading zones for passively loaded hormone; **(C)** Hormone flux in the loading/unloading zones for actively loaded hormone; **(D)** Phloem transport velocity; **(E)** Sugar concentration; **(F)** Hormone concentration for a passively loaded hormone; **(G)** Hormone concentration for an actively loaded hormone. **Sugar parameter values:** as given in Table 1 with additional variations to $(\sigma_{s,1}, \sigma_{s,2}, \sigma_{s,3}) = (1, 1, \text{varied})$. **Auxin parameter values:** as given in Table 2 with additional variations to $(\sigma_{a,1}, \sigma_{a,2}, \sigma_{a,3}) = (1, 1, \text{varied})$. **Mü** = 0.22. Simulations of model equations (18).

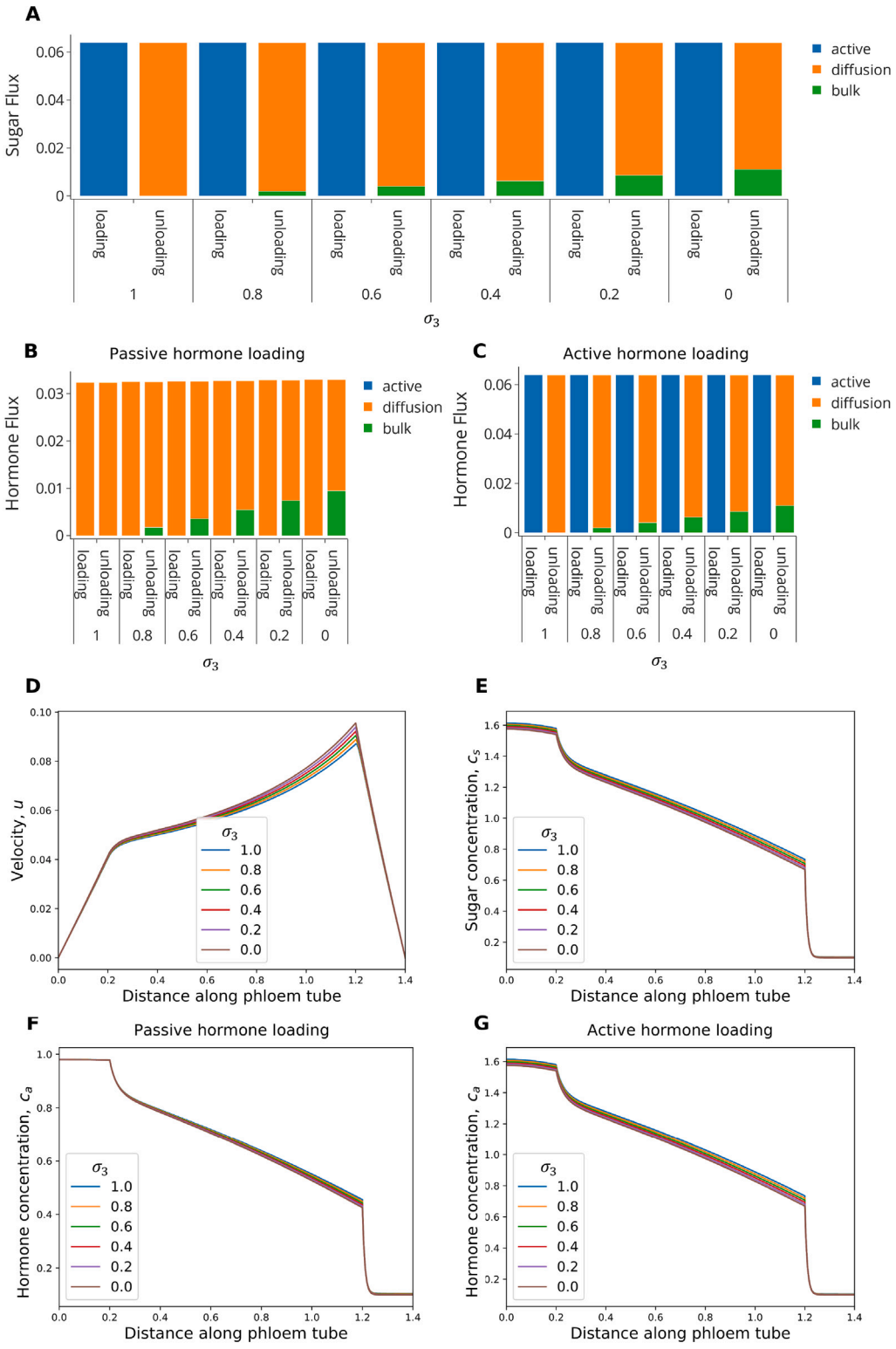

Fig. 4. Results showing how a larger Münch number impacts the results of varying the Staverman reflection coefficient for sugar and hormone. Velocity and concentration profiles vary in shape from Fig. 3 but impact of varying $\sigma_{s,3}/\sigma_{a,3}$ remains consistent. **(A)** Sugar flux in the loading/unloading zones; **(B)** Hormone flux in the loading/unloading zones for passively loaded hormone; **(C)** Hormone flux in the loading/unloading zones for actively loaded hormone; **(D)** Phloem transport velocity; **(E)** Sugar concentration; **(F)** Hormone concentration for a passively loaded hormone; **(G)** Hormone concentration for an actively loaded hormone. **Sugar parameter values:** as given in Table 1 with additional variations to $(\sigma_{s,1}, \sigma_{s,2}, \sigma_{s,3}) = (1, 1, \text{varied})$. **Auxin parameter values:** as given in Table 2 with additional variations to $(\sigma_{a,1}, \sigma_{a,2}, \sigma_{a,3}) = (1, 1, \text{varied})$. **Mü** = 12.

Table 5
Sugar parameters values around which variations are performed to yield simulations in the following sections (bulk flow unloading dominates over diffusive unloading).

Parameter group	Default values	Parameter description
$(\sigma_{s,1}, \sigma_{s,2}, \sigma_{s,3})$	(1, 1, 0.2)	Bulk flow
$(\beta_{s,1}, \beta_{s,2}, \beta_{s,3})$	(0, 0, 1)	Passive diffusion
$(\gamma_{s,1}, \gamma_{s,2}, \gamma_{s,3})$	(0.16, 0, 0)	Active loading
$(\lambda_{s,1}, \lambda_{s,2}, \lambda_{s,3})$	(0, 0, 0)	Active unloading
$(C_{ext,s,1}, C_{ext,s,2}, C_{ext,s,3})$	(1, 0, 0.4)	External sugar concentration

Table 6
Hormone parameter values around which variations are performed to yield simulations in the following sections (bulk flow unloading of hormone dominates over diffusive unloading).

Parameter group	Passive hormone loading	Active hormone loading
$(\sigma_{a,1}, \sigma_{a,2}, \sigma_{a,3})$	(1, 1, 0.2)	(1, 1, 0.2)
$(\beta_{a,1}, \beta_{a,2}, \beta_{a,3})$	(5*, 0, 1)	(0, 0, 1)
$(\gamma_{a,1}, \gamma_{a,2}, \gamma_{a,3})$	(0, 0, 0)	(0.16, 0, 0)
$(\lambda_{a,1}, \lambda_{a,2}, \lambda_{a,3})$	(0, 0, 0)	(0, 0, 0)
$(C_{ext,a,1}, C_{ext,a,2}, C_{ext,a,3})$	(1, 0, 0.4)	(1, 0, 0.4)

With a fixed rate of active sugar loading, $\gamma_{s,1}$, increasing the ratio between the root and shoot external sugar concentrations, $C_{ext,s,3}$, results in a larger parameter region where bulk flow unloading is dominant over diffusive unloading (Fig. 5). In contrast, with a fixed external sugar concentration in the unloading zone, $C_{ext,s,3}$, we see that varying the rate of active sugar loading, $\gamma_{s,1}$, has little impact on the amount of unloading occurring via bulk flow (Fig. 6). We note that the influence of these parameters and physical interpretations are detailed in Sections 4.4 and 4.5.

In cases where bulk flow unloading is dominant and the rate of diffusion, $\beta_{s,3}$ is small, the model can predict an accumulation of sugar in the unloading zone – a characteristic not currently described in the literature (Figs. 5 and 6). This is likely due to the rate of diffusion being too low to allow the model to meet the prescribed rate of unloading flux (which is fixed for each set of simulations as we fix $\gamma_{s,1}$) without producing an extremely high concentration difference across the membrane in the unloading zone. However, there are parameter regions where bulk flow unloading is dominant and no sugar accumulation occurs (for example, if $C_{ext,s,3}$ is sufficiently large, Fig. 5E).

In summary, the model predicts that bulk flow unloading can be dominant over diffusive unloading. The simulations suggest that for bulk flow to dominate requires a small Staverman reflection coefficient, $\sigma_{s,3}$, and a large ratio between the root and shoot external sugar concentrations, $C_{ext,s,3}$. Although the model predicts accumulation of sugar in the phloem unloading zone for some parameter regimes, it is not clear whether such sugar accumulation occurs in the unloading zone of plants such as Arabidopsis. Hence, for the remaining simulation results presented, we set model parameters such that bulk flow unloading dominates over diffusive unloading, but with a sugar concentration profile that is consistent with those in the theoretical literature (Jensen et al., 2012; Payvandi et al., 2014), see Table 5. As hormones are smaller molecules than sugar, we assume that the hormone parameters are consistent with those specified for sugar (although with either diffusive or active loading), Table 6.

4.4. Increasing active sugar loading increases phloem transport velocity and increases the rate of delivery of passively loaded hormones

Abiotic stresses, such as drought, heat stress, light intensity, and temperature have been shown to impact sucrose transporters and phloem loading in a range of plants, including Arabidopsis, maize, and wheat Xu et al. (2018), Knox et al. (2018), Gong et al. (2015). Active sugar loading occurs via SUC transporters and varying the rate of active sugar loading, $\gamma_{s,1}$, in the model is consistent with the relative expression levels of SUC transporters changing according to environmental conditions (Xu et al., 2018; Knox et al., 2018; Gong et al., 2015). We investigate how these responses to environmental cues impact hormone delivery to the root tip.

Increasing the rate of active sugar loading, $\gamma_{s,1}$, increases the total sugar loading and unloading (Fig. 7A) (recalling that at the steady state the total loading and unloading are equal). An increase in the rate of active sugar loading is predicted to result in an increased phloem transport velocity (Fig. 7D), consistent with experimental results from Knox et al. (2018), and an increase in sugar concentration throughout the phloem (Fig. 7E), consistent with experimental measurements of sucrose concentration within phloem exudate by Xu et al. (2018). Interestingly, as the sugar loading rate is increased, the proportion of unloading that occurs via diffusive unloading increases (Fig. 7A) (which is consistent with the parameter survey shown in Fig. 6). The increase in diffusive unloading occurs as there is an increase in sugar phloem concentration in the unloading zone which increases the gradient down which diffusive unloading occurs (Fig. 7E).

As for bulk flow unloading (varying σ_s), increasing active sugar loading also affects hormone delivery. For passively loaded hormones, increasing the rate of active sugar loading increases phloem transport velocity which in turn decreases the hormone concentration in the loading zone. This increases the concentration difference across the membrane in the loading zone which leads to an increase in passive loading. Due to the steady-state nature of our model, this increases the amount of hormone delivered to the root tip (Fig. 7B, F). For actively loaded hormones (Fig. 7C, G), the proportion of unloading that occurs via bulk flow increases as the rate of active sugar loading is increased (due reduced hormone concentrations in the unloading zone decreasing the concentration difference which drives diffusive unloading). These cases suggests that environmental conditions that impact SUC-mediated active sugar transport in the shoot, such as changes in light intensity (Xu et al., 2018; Knox et al., 2018), can influence hormone delivery in the root tip via changes to the phloem transport velocity.

In summary, increasing active sugar loading results in increased phloem transport velocities which influences hormone delivery to the root tip. In the case of actively loaded hormones, the model predicts a shift in the dominant unloading mechanism, whereas for passively loaded hormones, the model predicts an increase in hormone delivery to the root tip.

4.5. Increasing the ratio between root and shoot external tissue sugar concentrations has little impact on the unloading of hormones

Modifications to the ratio between root and shoot external sugar concentrations, $C_{ext,s,3}$, can occur either by changes at the shoot or changes at the root. For example, application of exogenous sucrose to the root tip increases the root:shoot external sugar concentration ratio and has been shown to reduce phloem transport velocity (Knox et al., 2018). Understanding how application of exogenous sucrose impacts phloem transport is important because some experiments incorporate sucrose into the growth medium, which could influence hormone delivery to the root tip. Another method of modifying the root:shoot external sugar concentration ratio is via changes in environmental conditions that lead to sugar accumulation in leaves (Xu et al., 2018) which increases the sugar concentration in the source tissues and would decrease the root:shoot external sugar concentration ratio.

The model predicts a reduction in phloem transport velocity for higher $C_{ext,s,3}$ (Fig. 8D), as observed in experimental studies by Knox et al. (2018). We note that as the ratio $C_{ext,s,3}$ approaches 1, we expect the phloem transport velocity to approach zero as there is no concentration gradient to drive phloem flow. An increase in $C_{ext,s,3}$ is predicted to lead to a higher sugar concentration in the phloem, seen most notably in the unloading zone (Fig. 8E). The model predicts that increasing $C_{ext,s,3}$ decreases the amount of diffusive sugar unloading and increases the relative contribution of the bulk flow sugar unloading (Fig. 8A). Increasing $C_{ext,s,3}$ reduces diffusive unloading by reducing the

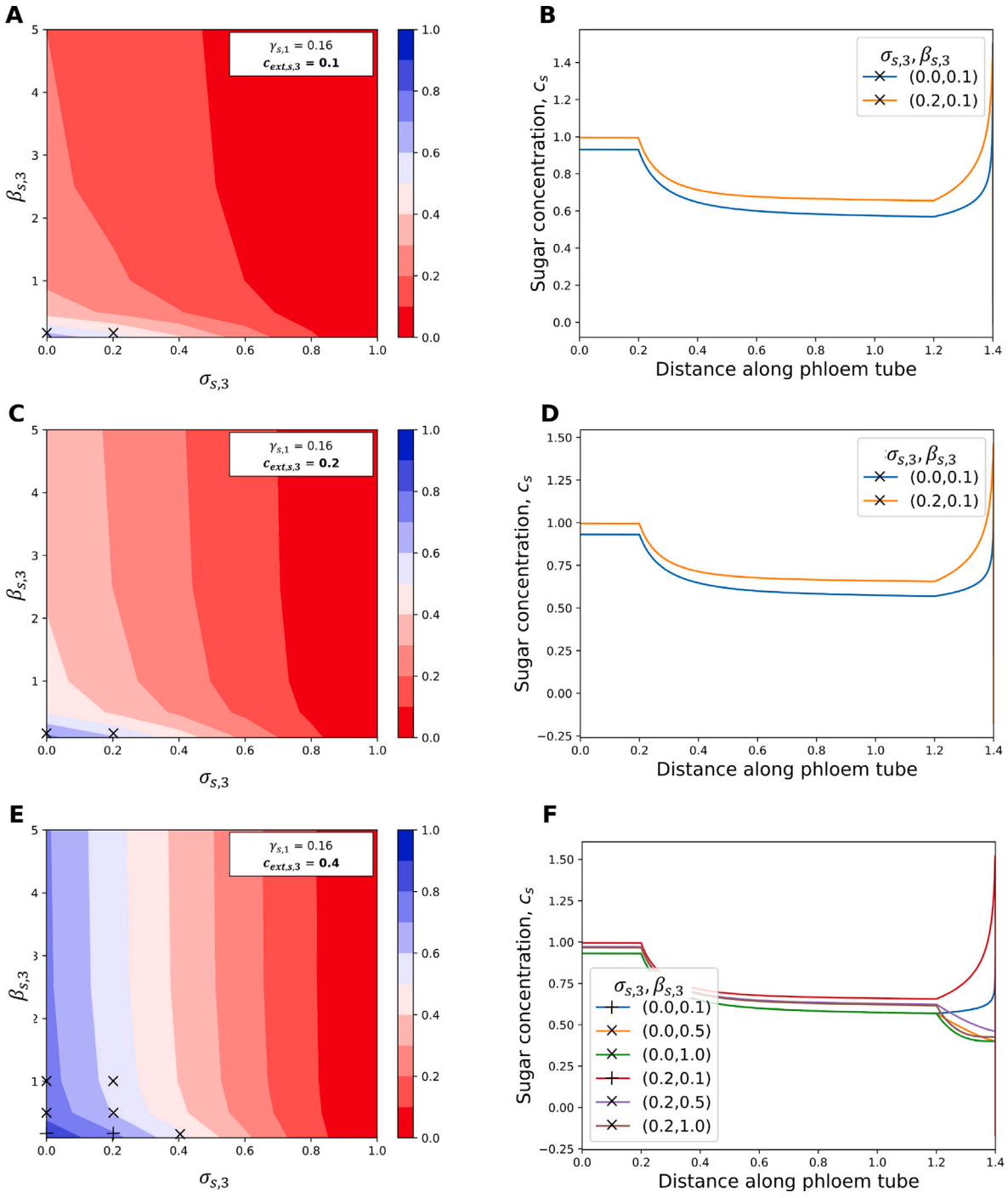

Fig. 5. Larger external sugar concentration in the unloading zone results in more bulk flow unloading. **(A/C/E)** Contour plots show the fraction of unloading that occurs via bulk flow. Blue shades indicate bulk flow unloading is dominant, red shades indicate diffusive unloading is dominant. Markers show parameter sets plotted in B/D/F – crosses indicate there is sugar accumulation in the unloading zone, pluses indicate sugar decreases in the unloading zone. **(B/D/F)** Parameter regimes that result in bulk flow unloading being dominant.

sugar concentration difference between the phloem and the external tissue.

For both hormone loading scenarios, we see an increase in the phloem hormone concentration as phloem transport velocity is decreased by an increase in $C_{ext,s,3}$ (Figs. 8F & G). This is consistent with results in Figs. 7 D, F & G and discussed in Section 4.4.

In summary, increasing the ratio between root and shoot external sugar concentrations, $C_{ext,s,3}$, reduces the phloem transport velocity which is consistent with experimental results from Knox et al. (2018). Whilst changes to $C_{ext,s,3}$ do modify phloem transport velocity, the impact is less pronounced than changes seen when changing $\gamma_{s,1}$, and as such the impact on the unloading of hormone is less pronounced. In the

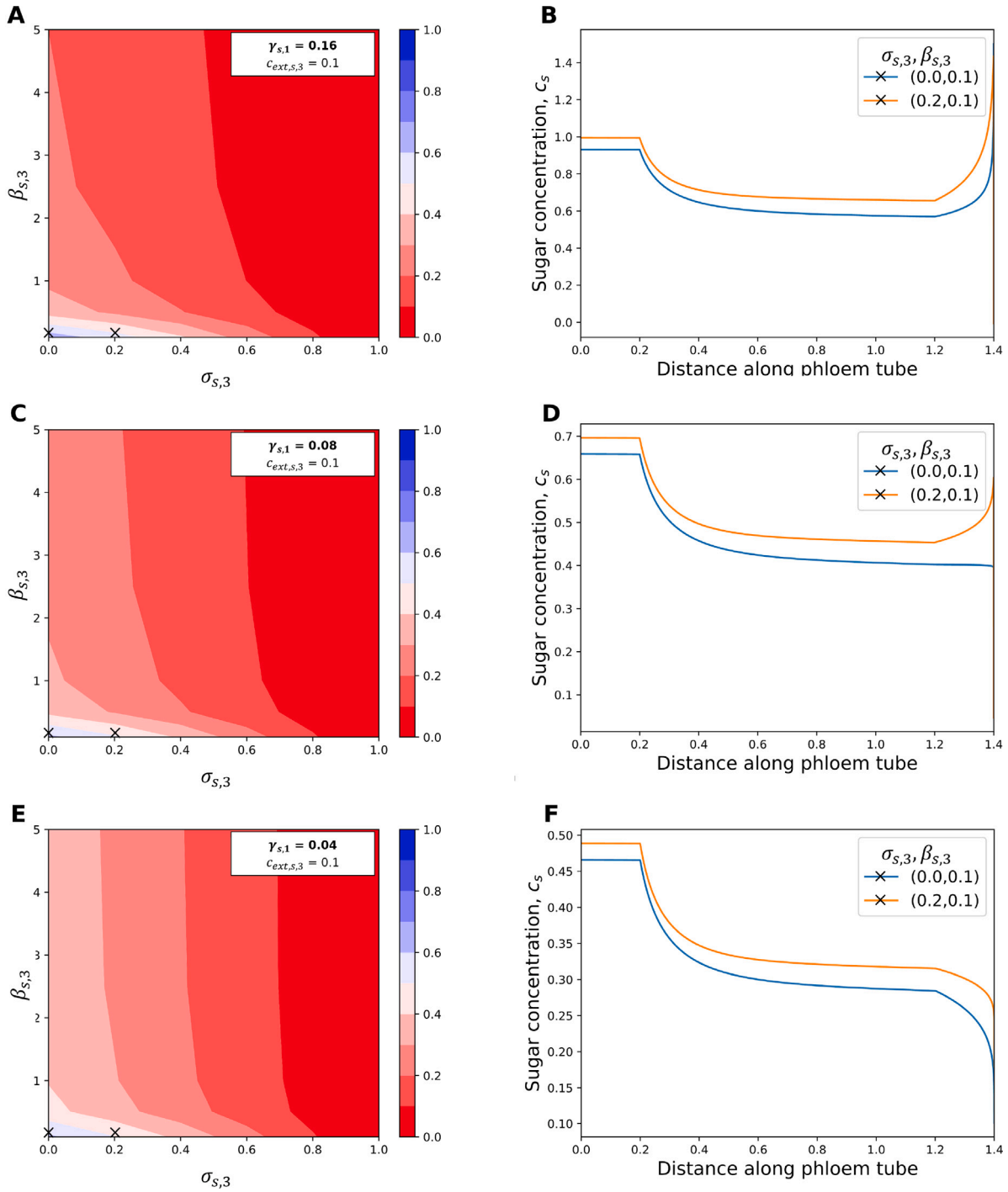

Fig. 6. Varying active sugar loading has little impact of the dominant form of unloading (which remains diffusive). **(A/C/E)** Contour plots show the fraction of unloading that occurs via bulk flow. Blue shades indicate bulk flow unloading is dominant, red shades indicate diffusive unloading is dominant. Markers show parameter sets plotted in B/D/F – crosses indicate there is sugar accumulation in the unloading zone, pluses indicate sugar decreases in the unloading zone. **(B/D/F)** Parameter regimes that result in bulk flow unloading being dominant.

case of passively loaded hormones, the model predicts that changing $C_{ext,s,3}$ has minimal impact on hormone delivery to the root tip.

4.6. Varying plasmodesmata density modifies phloem transport velocity

Unloading via diffusion and bulk flow occurs through plasmodesmata. As such, environmental conditions that influence plasmodesmata transport rates or plasmodesmata density will have an effect on the unloading dynamics in the model. Transport via plasmodesmata has been shown to be affected by light levels and the circadian clock (Brunkard and Zambryski, 2019), as well as osmotic stress and cold stress (Sager and Lee, 2014 and references therein).

Changes in plasmodesmata transport rates or plasmodesmata density will affect unloading via both diffusion and bulk flow. As such, to model environmental changes that impact plasmodesmata, we need to vary the diffusion coefficients for sugar and hormone, $\beta_{s,3}, \beta_{a,3}$, as well as the Staverman reflection coefficients for sugar and hormone, $\sigma_{s,3}, \sigma_{a,3}$. Increasing $\beta_{s,3}, \beta_{a,3}$ and decreasing $\sigma_{s,3}, \sigma_{a,3}$ can be considered

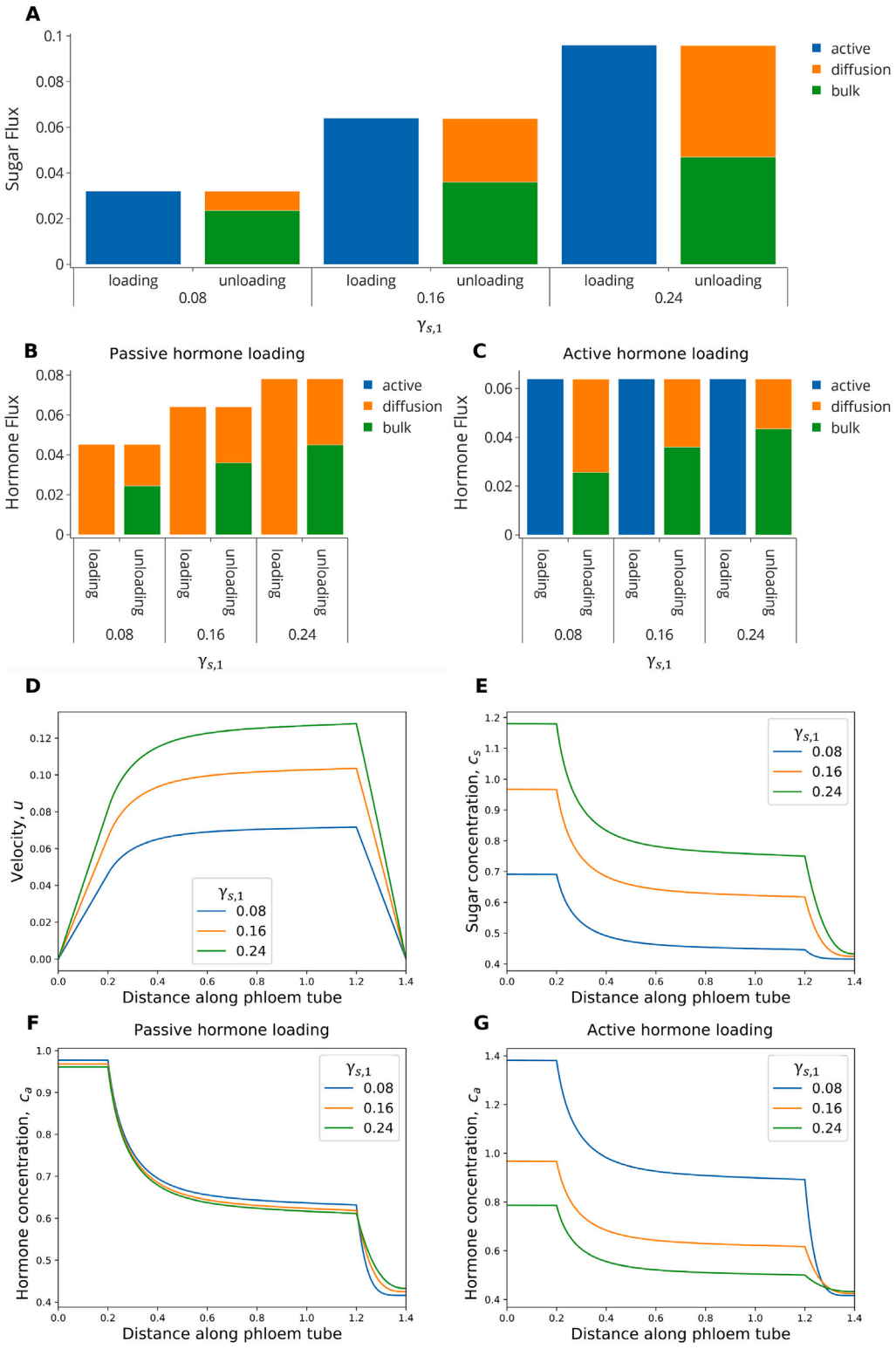

Fig. 7. Increasing active sugar loading results in a change in the dominant form of hormone unloading, shifting from diffusion dominant to bulk flow dominant as $\gamma_{s,1}$ increases. This occurs alongside an increase to phloem transport velocity. **(A)** Sugar flux in the loading/unloading zones; **(B)** Hormone flux in the loading/unloading zones for passively loaded hormone; **(C)** Hormone flux in the loading/unloading zones for actively loaded hormone; **(D)** Phloem transport velocity; **(E)** Sugar concentration; **(F)** Hormone concentration for a passively loaded hormone; **(G)** Hormone concentration for an actively loaded hormone. **Sugar parameter values:** as given in Table 5 with additional variations to $(\gamma_{s,1}, \gamma_{s,2}, \gamma_{s,3}) = (\text{varied}, 0, 0)$. **Auxin parameter values:** as given in Table 6. **Mü** = 0.22.

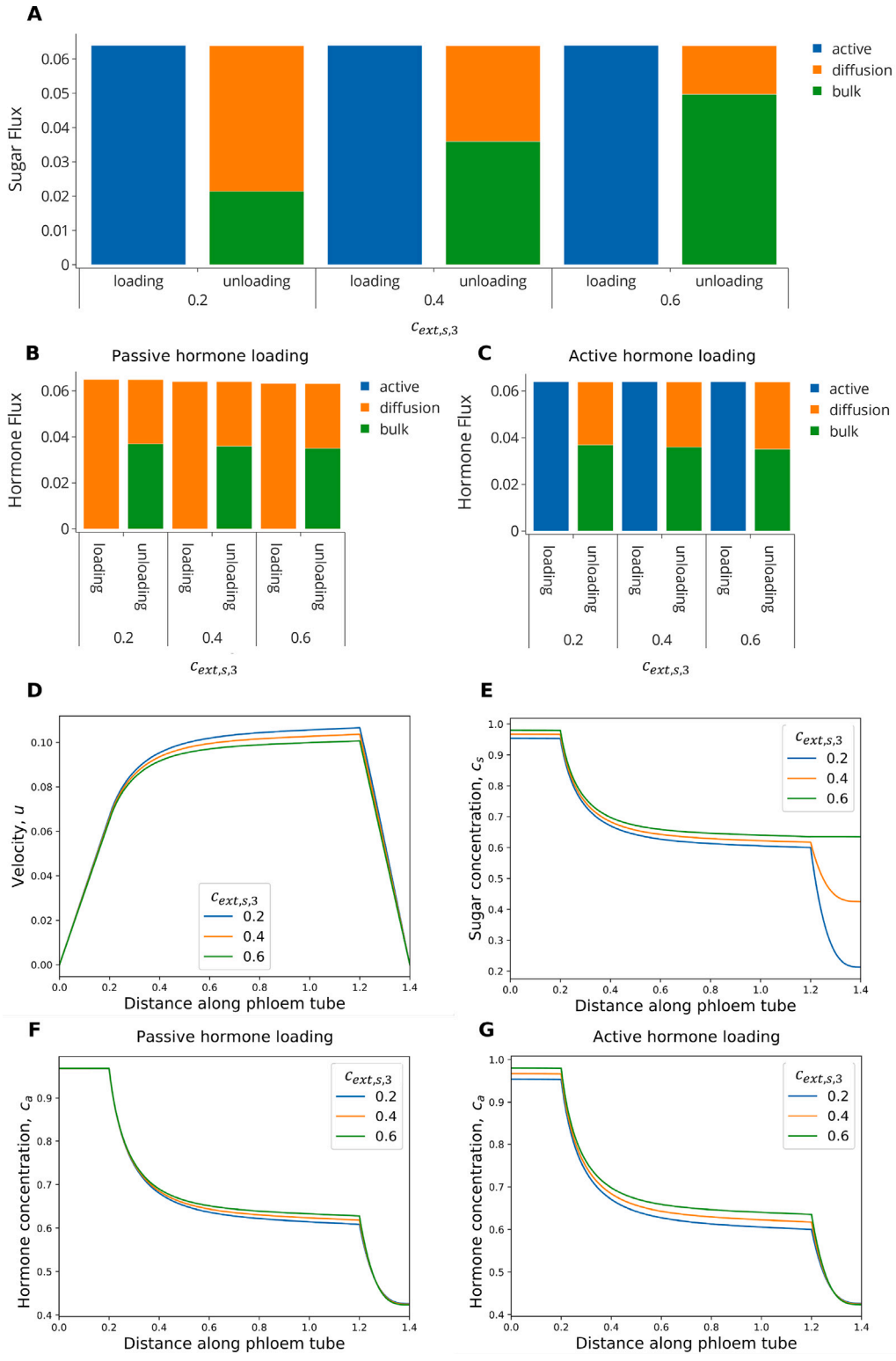

Fig. 8. Reducing sugar sink strength by increasing $C_{ext,s,3}$ has little impact on the unloading dynamics of hormones. **(A)** Sugar flux in the loading/unloading zones; **(B)** Hormone flux in the loading/unloading zones for passively loaded hormone; **(C)** Hormone flux in the loading/unloading zones for actively loaded hormone; **(D)** Phloem transport velocity; **(E)** Sugar concentration; **(F)** Hormone concentration for a passively loaded hormone; **(G)** Hormone concentration for an actively loaded hormone. **Sugar parameter values:** as given in Table 5 with additional variations to $(C_{ext,s,1}, C_{ext,s,2}, C_{ext,s,3}) = (1, 0, \text{varied})$. **Auxin parameter values:** as given in Table 6. **Mü** $= 0.22$.

Table 7
Parameter variations used for model scenarios of low, mid, and high plasmodesmata density.

Plasmodesmata density	$\sigma_{s,3}, \sigma_{a,3}$	$\beta_{s,3}, \beta_{a,3}$
Low	0.3	0.5
Mid	0.2	1.0
High	0.1	1.5

to represent an increase in plasmodesmata transport rate or an increase in plasmodesmata density. In the following simulations, as we are varying multiple parameters simultaneously, we label the simulations as low, mid, and high to represent a scale from decreased to increased plasmodesmatal transport. Parameter values used in each scenario are given in Table 7 and correspond to the region shown in Fig. 9A.

For parameters in Table 6, increasing plasmodesmatal unloading is predicted to increase the contribution of bulk flow unloading (Figs. 9B, C, D). However, it is important to note that this relationship is not well-defined and that alternative definitions of low, mid, and high plasmodesmata density could alter the proportion of unloading that occurs via bulk flow. This is seen most clearly in the curved nature of the contours in Fig. 9A. For example, an alternative high plasmodesmata density scenario could be $\sigma_{s,3} = 0.175$, $\beta_{s,3} = 1.2$ which would give bulk flow as a fraction of unloading comparable to our current low and mid density scenarios. As such, further investigation is needed to accurately define the relationship between plasmodesmata density and model parameters $\sigma_{s,3}$ and $\beta_{s,3}$.

Increasing plasmodesmatal transport results in an increase in phloem transport velocity (Fig. 9E) and a corresponding decrease in phloem sugar concentration (Fig. 9F). Consistently with the previous results (Fig. 7), the increased velocity results in a reduction in hormone concentration in the loading zone, which results in an increase of hormone delivery for passively loaded hormones (Fig. 9C). Increased phloem transport velocity also leads to a decrease in phloem hormone concentration in both loading scenarios (Figs. 9G, H). Whilst changes in phloem transport velocity might lead to small changes in the dominant form of hormone unloading, the changes in the contribution to bulk flow unloading seen in Figs. 9 C and D are most likely caused by the specific changes in hormone parameters associated with plasmodesmata density (Table 7).

In summary, the model suggests that increasing plasmodesmata density results in an increase in phloem transport velocity which in turns leads to increased hormone delivery to the root tip for passively loaded hormones.

5. Conclusions

In this paper, we have developed a mathematical model for plant hormone transport via the phloem that couples the hormone and sugar dynamics. This model builds upon the work of Jensen et al. (2012, 2016), Payvandi et al. (2014), extending existing models in the literature to incorporate hormone transport, bulk flow unloading, and more physical loading/unloading mechanisms.

Focusing on actively loaded sugar, the model predicts that increasing bulk flow sugar unloading or increasing the rate of active sugar loading both increase the phloem transport velocity. For passively loaded hormones, increases in phloem transport velocity are predicted to increase the amount of hormone delivered to the root tip. In contrast, for actively loaded hormone, the model shows that the total hormone delivery is independent of the sugar dynamics and phloem velocity. This is because active loading is independent of phloem hormone concentration, and at steady state the rate of loading must equal the rate of unloading.

Surveying parameter space, we identified regions where bulk flow unloading of sugar dominates over diffusive unloading as suggested by Ross-Elliott et al. (2017), finding this is predominantly influenced by the choice of a small Staverman reflection co-efficient and a large ratio between shoot and root external sugar concentrations. Although the root-to-shoot external sugar concentration ratio has a substantial influence on the proportion of bulk flow unloading, the model predicts that increasing this ratio leads to only a small reduction in the phloem transport velocity and limited impact on hormone delivery to the root tip.

The model provides key insights into how environmental conditions that affect the sugar dynamics lead to changes in hormone delivery to the root tip. Active sugar loading is influenced by numerous environmental conditions. The model predictions align with experimental data (such as changes in light intensity and temperature Xu et al., 2018; Knox et al., 2018) that suggest that increasing active sugar loading increases phloem transport velocity and phloem sugar concentration. Furthermore, the model predicts that an increase in active sugar loading will increase hormone delivery to the root tip for passively loaded hormones. In contrast, environmental changes that increase the ratio between root and shoot external sugar concentration (such as the inclusion of exogenous sucrose in growth medium Knox et al., 2018) are predicted to lead to only a small decrease in the phloem velocity and little influence on hormone delivery.

Environmental conditions also influence plasmodesmatal densities and permeabilities and thus, the rates of passive unloading (both diffusive and bulk flow unloading). The model predicts that a higher plasmodesmatal density results in a larger phloem transport velocity, and thus increases the hormone delivery to the root tip for passively loaded hormones.

Overall, our model highlights the important role that sugar dynamics can have on hormone delivery to the root tip. As highlighted above, the model is qualitatively consistent with experimental results in the literature on phloem velocity and sugar transport. However, quantitative comparisons are not currently possible as many of the parameter values have not been experimentally determined (for example, bulk flow unloading rates have not been determined in any model species). Furthermore, we are not aware of any experimental data on hormone transport in the phloem that would enable quantitative comparison with our model predictions. Future modelling work could focus on extending the model described here to capture dynamic changes in the source/sink concentration levels. Furthermore, by deriving the model for general axial-position-dependent external concentration levels our work can be easily extended to scenarios where there are multiple loading/unloading zones, such as unloading of sugar and hormones within growing leaves as well as at root tissues.

CRediT authorship contribution statement

Heather L. Collis: Conceptualization, Methodology, Software, Validation, Formal analysis, Writing – original draft. **Markus R. Owen:** Conceptualization, Methodology, Writing – review & editing, Supervision, Funding acquisition. **Leah R. Band:** Conceptualization, Methodology, Writing – review & editing, Supervision.

Declaration of competing interest

The authors declare that they have no known competing financial interests or personal relationships that could have appeared to influence the work reported in this paper.

Data availability

Python code that produces each of the simulations is available at https://gitlab.com/leahband/phloem_hormone_model.

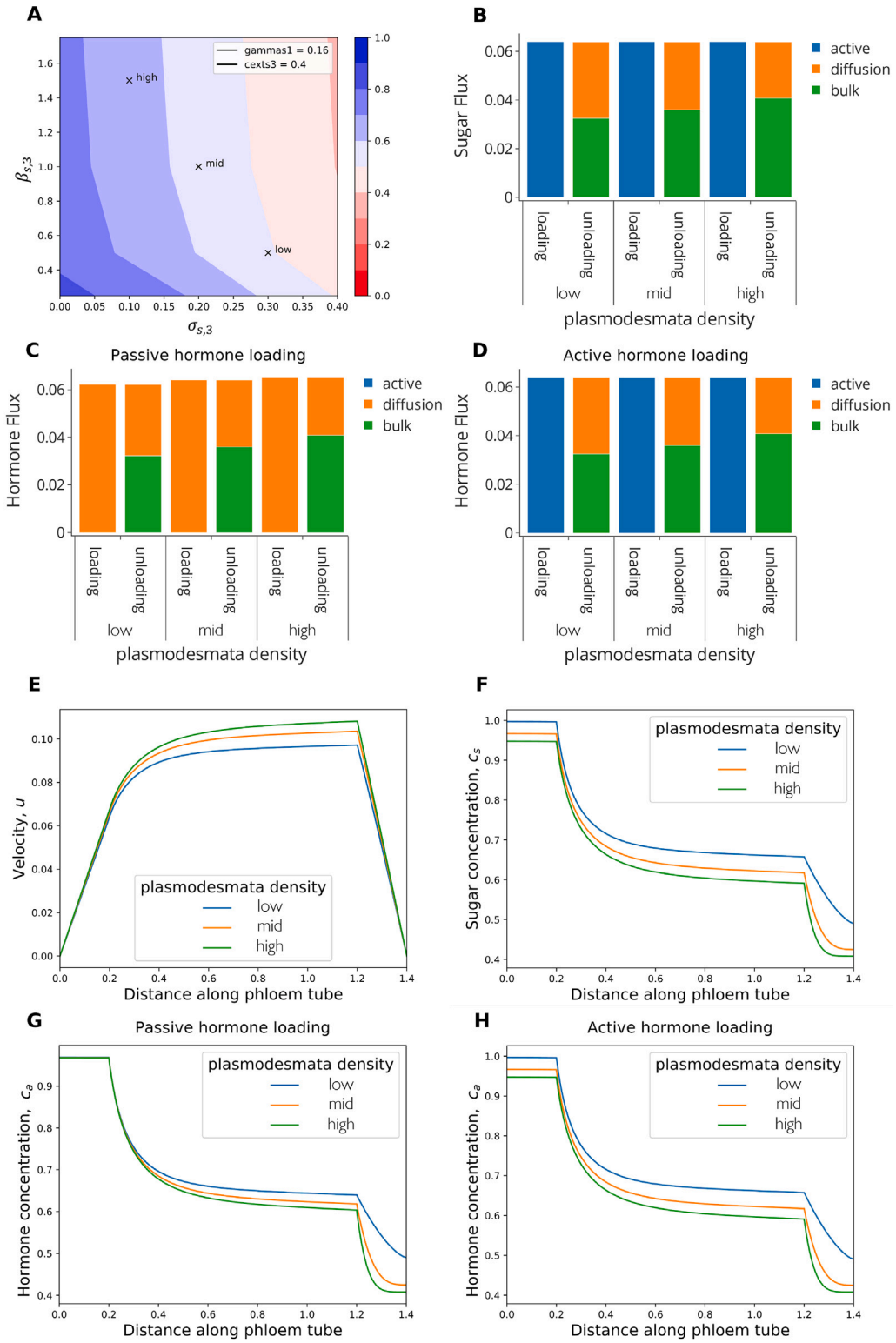

Fig. 9. **(A)** Contour plot showing parameter region in which low, mid, and high plasmodesmata density scenarios are located. (Contour plots show the fraction of unloading that occurs via bulk flow. Blue shades indicate bulk flow is dominant, red shades indicate diffusive unloading is dominant.); **(B)** Sugar flux in the loading/unloading zones; **(C)** Hormone flux in the loading/unloading zones for passively loaded hormone; **(D)** Hormone flux in the loading/unloading zones for actively loaded hormone; **(E)** Phloem transport velocity; **(F)** Sugar concentration; **(G)** Hormone concentration for a passively loaded hormone; **(H)** Hormone concentration for an actively loaded hormone. **Sugar parameter values:** as given in Table 5 with additional variations to $(\beta_{s,1}, \beta_{s,2}, \beta_{s,3}) = (1, 0, \text{varied})$ and $(\sigma_{s,1}, \sigma_{s,2}, \sigma_{s,3}) = (1, 0, \text{varied})$. **Auxin parameter values:** as given in Table 6 with additional variations to $(\beta_{a,1}, \beta_{a,2}, \beta_{a,3}) = (1, 0, \text{varied})$ and $(\sigma_{a,1}, \sigma_{a,2}, \sigma_{a,3}) = (1, 0, \text{varied})$. **Mü** $= 0.22$.

Table 8
Diffusion coefficients for a range of plant hormones calculated using the Stokes–Einstein equation (the diffusion coefficient for auxin is cited from Kramer and Went, 1949).

Hormone	Diffusion coefficient ($m^2\ s^{-1}$)
Auxin	6.7×10^{-10} (Kramer and Went, 1949)
Cytokinin	6.2×10^{-10}
Brassinosteriods	4.4×10^{-10}
Gibberellin	5.4×10^{-10}

Acknowledgments

This work was supported by the Leverhulme Trust Doctoral Scholarships programme (grant number DA214-024). We thank Prof Malcolm Bennett and Prof Michael Knoblauch for helpful discussions.

Appendix A. Stokes–Einstein calculations for plant hormone diffusion coefficients

Here, we investigate the timescales for diffusion, advection, and growth, as well as the Péclet number, for sugar and a range of hormones. In order to do this we require various parameters including $D_s = 5.0 \times 10^{-10}\ m^2 s^{-1}$, the diffusivity coefficient of sugar (Gosting and Morris, 1949); $\bar{u} = 23\ \mu m s^{-1}$, the sap flow speed (Ross-Elliott et al., 2017); $RER = 3.6 \times 10^{-4}\ mh^{-1}$, the root elongation rate for *Arabidopsis*; $L = 30.6$ mm, the primary root length of an *Arabidopsis* seedling 7DAG (Martin et al., 2002); and the diffusivity coefficients for a range of hormones.

As the diffusion coefficients for some hormones are not available in the literature, we calculate them using the Stokes–Einstein equation (Truskey et al., 2010b),

$$D = \frac{k_B T}{6\pi\mu}\left(\frac{4\pi N_A}{3\bar{v}M}\right)^{\frac{1}{3}}, \tag{23}$$

where D is the diffusion coefficient of the hormone to be determined, k_B is the Boltzmann constant, T is the absolute temperature, μ is viscosity of water, N_A is Avogadro's number, $\bar{v}$ is the specific volume of the hormone (given by the inverse of its density), and M is the molecular weight of the hormone. Table 8 shows the derived diffusion coefficients for the hormones we consider.

Table 9 gives the values used in these calculations and their corresponding references.

From Table 10, we can see that we have large Péclet number for our hormones and sugar. Therefore, we assume advection is dominant and can neglect diffusion terms. The timescale of growth is also much slower than transport timescales, this justifies our use of the steady state equations.

Appendix B. Shooting method

The shooting method requires us to convert the boundary value problem in Eqs. (18) to an initial-value problem. We then solve the initial-value problem to find a solution for a given initial condition and then feed the solution into an iteration formula that allows us to correct the initial condition until we obtain a result that satisfies our second boundary condition. We use the initial condition,

$$\frac{\partial \bar{U}}{\partial X}(0) = t, \tag{24a}$$

where t is a constant that needs to be determined. The term t is called our shooting parameter. We then solve this system to find a solution which we denote $\bar{U}(X;t)$. Our aim is to find a value for t such that $\bar{U}(X_3;t) = 0$. To do this, we first solve the initial-value problem for two initial estimates for t, t_1 and t_2, such that $\bar{U}(X_3;t_1) > 0$ and $\bar{U}(X_3;t_2) < 0$. We then use the bisection method to calculate $t_3 = {}^{(t_1+t_2)}/_2$ and then solve the initial-value problem for t_3. If $\bar{U}(X_3;t_3) > 0$ we replace t_1 with t_3, and if $\bar{U}(X_3;t_3) < 0$ we replace t_2 with t_3. We repeat this process until $|\bar{U}(X_3;t)| < 10^{-6}$, at which point we consider our system solved.

Appendix C. Upwind scheme for numerical simulations

In this section, we seek numerical solutions to our full phloem model. The Eqs. (18) can be rewritten for numerical simulation using an Upwind Scheme (Jensen et al., 2012). We divide the length of our phloem tube into a set of discrete points $X_n = (n-1)\Delta X$, $n = 1, \dots, N$, where $\Delta X = X_3/(N-1)$, and use the following approximations for the differential terms,

$$\frac{\partial \bar{U}}{\partial X}(X_j) \simeq \frac{\bar{U}(X_j) - \bar{U}(X_{j-1})}{\Delta X}, \tag{25}$$

$$\frac{\partial C_s}{\partial X}(X_j) \simeq \frac{C_s(X_j) - C_s(X_{j-1})}{\Delta X}, \tag{26}$$

$$\frac{\partial C_a}{\partial X}(X_j) \simeq \frac{C_a(X_j) - C_a(X_{j-1})}{\Delta X}, \tag{27}$$

$$\frac{\partial P}{\partial X}(X_j) \simeq \frac{P(X_j) - P(X_{j-1})}{\Delta X}. \tag{28}$$

With the notation $\bar{U}_j = \bar{U}(X_j)$, and similarly for C_s, C_a and P, these approximations can be substituted into (18) to obtain our numerical model,

$$\bar{U}_j = \bar{U}_{j-1} + \sigma_{s,j}\Delta X(C_{s,j-1} - C_{x,s,j-1}) - \frac{M\ddot{u}}{8}\Delta X(P_{j-1} - P_{x,j-1}) \tag{29a}$$

$$P_j = P_{j-1} - 8\Delta X\bar{U}_j, \tag{29b}$$

$$C_{s,j} = \frac{-B_s \pm \sqrt{B_s^2 + 4A_s D_s}}{2A_s}, \tag{29c}$$

$$C_{a,j} = \frac{\bar{U}_j C_{a,j-1} + \left[\frac{(1-\sigma_{a,j})}{2}\left(\sigma_{s,j}(C_{s,j} - C_{x,s,j}) - \frac{M\ddot{u}}{8}(P_j - P_{x,j})\right) + 2(\beta_{a,j} + \gamma_{a,j})\right]C_{ext,a,j}\Delta X}{2\bar{U}_j - \bar{U}_{j-1} - \left[\frac{(1-\sigma_{a,j})}{2}\left(\sigma_{s,j}(C_{s,j} - C_{x,s,j}) - \frac{M\ddot{u}}{8}(P_j - P_{x,j})\right) - 2(\beta_{a,j} + \lambda_{a,j})\right]\Delta X}, \tag{29d}$$

where,

$$A_s = -\frac{\sigma_{s,j}(1-\sigma_{s,j})\Delta X}{2}, \tag{30a}$$

$$B_s = 2\bar{U}_j - \bar{U}_{j-1} + 2\Delta X(\beta_{s,j} + \lambda_{s,j}) + \frac{(1-\sigma_{s,j})\Delta X M\ddot{u}}{16}(P_j - P_{x,j}) - \frac{\sigma_{s,j}(1-\sigma_{s,j})\Delta X}{2}(C_{ext,s,j} - C_{x,s,j}), \tag{30b}$$

$$D_s = C_{s,j-1}\bar{U}_j + 2\Delta X(\beta_{s,j} + \gamma_{s,j})C_{ext,s,j} - \left[\frac{(1-\sigma_{s,j})\Delta X M\ddot{u}}{16}(P_j - P_{x,j}) + \frac{\sigma_{s,j}(1-\sigma_{s,j})\Delta X}{2}C_{x,s,j}\right]C_{ext,s,j}. \tag{30c}$$

In Eq. (29c), we take the root with the plus sign as this is always greater than zero. As A_s has a maximum order of 10^{-5} (when $\sigma_s = 0.5$), we can use the binomial expansion for small A_s to obtain an approximation for the sugar concentration equation, (29c), as,

$$C_{s,j} = \frac{D_s}{B_s} - A_s\frac{D_s^2}{B_s^3} + O(A_s^2). \tag{31}$$

Noticing that $A_s^2 = O(\Delta X^2)$ we can neglect the $O(A_s^2)$ terms in Eqs. (31) as terms of $O(\Delta X^2)$ are assumed negligible.

We solve the system of governing equations numerically in `Python 3.8`. The shooting parameter t is used to calculate values at X_2 from initial conditions defined at X_1 (see Appendix D for initial value definitions). The solutions can then be propagated forward in space (j) using Eqs. (29a), (29b), (29d), (30) and (31). The solution for $\bar{U}$ at X_N is then assessed by its distance from 0. This process is then iterated as described in Appendix B.

Table 9
Parameter values used in the calculation of plant hormone diffusivity coefficients using the Stokes–Einstein equation.

Parameter	Value	Unit	Reference
k_B	1.38×10^{-23}	kg m^2 s^{-2} K^{-1}	Truskey et al. (2010b)
T	298.15	K	Truskey et al. (2010b)
N_A	6.02×10^{23}	mol^{-1}	Truskey et al. (2010b)
μ	0.89×10^{-3}	kg m^{-1} s^{-1}	Truskey et al. (2010b)
$\bar{v}$ (Cytokinin)	0.714×10^{-3}	kg m^{-3}	ChemSpider, Royal Society of Chemistry (2021b)
$\bar{v}$ (Brassinosteriods)	0.909×10^{-3}	kg m^{-3}	ChemSpider, Royal Society of Chemistry (2021a)
$\bar{v}$ (Gibberellin)	0.667×10^{-3}	kg m^{-3}	ChemSpider, Royal Society of Chemistry (2021c)
M (Cytokinin)	219.1×10^{-3}	kg mol^{-1}	ChemSpider, Royal Society of Chemistry (2021b)
M (Brassinosteriods)	480.3×10^{-3}	kg mol^{-1}	ChemSpider, Royal Society of Chemistry (2021a)
M (Gibberellin)	346.1×10^{-3}	kg mol^{-1}	ChemSpider, Royal Society of Chemistry (2021c)

Table 10
Timescales of key transport processes and Péclet numbers.

Timescale	Formula	Value
Diffusion of sugar	L^2/D_s	520 h
Diffusion of auxin	L^2/D_a	388 h
Diffusion of cytokinin	L^2/D_a	420 h
Diffusion of brassinosteriods	L^2/D_a	591 h
Diffusion of gibberellin	L^2/D_a	482 h
Advection	$L/\bar{u}$	0.37 h
Growth	L/R_{ER}	85 h
$\mathrm{Pe}_{\mathrm{sugar}}$	$L\bar{u}/D_s$	1408
$\mathrm{Pe}_{\mathrm{auxin}}$	$L\bar{u}/D_a$	1050
$\mathrm{Pe}_{\mathrm{cytokinin}}$	$L\bar{u}/D_a$	1135
$\mathrm{Pe}_{\mathrm{brassinosteriods}}$	$L\bar{u}/D_a$	1600
$\mathrm{Pe}_{\mathrm{gibberellin}}$	$L\bar{u}/D_a$	1303

Appendix D. Initial values for numerical simulations

In order perform our numerical simulations, we require values for $C_s(0), C_a(0)$, and $P(0)$. Expanding the left-hand-side of Eq. (18b), rearranging for $\bar{U}\frac{\partial C_s}{\partial X}$, and evaluating at $X = 0$, we see that

$$(1-\sigma_s(0))\bar{C}_s(0)\left(\sigma_s(0)(C_s(0)-C_{x,s}(0)) - \frac{\mathrm{M\ddot{u}}}{8}(P(0)-P_x(0))\right) + 2(\beta_s+\gamma_s) - 2(\beta_s+\lambda_s) - C_s(0)\frac{\partial \bar{U}(0)}{\partial X} = 0. \tag{32}$$

Upon substitution of $\bar{C}_s(0)$, this yields a quadratic equation for the concentration of sugar at $X = 0$, $C_s(0)$.

Evaluating Eq. (18a) at $X = 0$, we can rearrange for $P(0)$, which gives,

$$P(0) = \frac{8}{\mathrm{M\ddot{u}}}\left(\sigma_s(0)(C_s(0)-C_{x,s}) - t\right) + P_x, \tag{33}$$

recalling that $\frac{\partial \bar{U}}{\partial X}(0) = t$ is our shooting parameter. Substituting $P(0)$ into Eq. (32), we obtain,

$$C_s(0) = \frac{\left(\frac{1-\sigma_s(0)}{2}t + 2(\beta_s+\gamma_s)\right)C_{ext,s}}{\left(1-\frac{1-\sigma_s(0)}{2}\right)t + 2(\beta_s+\lambda_s)} \tag{34}$$

Using the same approach, we obtain $C_a(0)$,

$$C_a(0) = \frac{\left(\frac{1-\sigma_a(0)}{2}t + 2(\beta_a+\gamma_a)\right)C_{ext,a}}{\left(1-\frac{1-\sigma_a(0)}{2}\right)t + 2(\beta_a+\lambda_a)} \tag{35}$$

Thus, we have obtained the initial values for $C_s(0)$, $C_a(0)$, and $P(0)$ in terms of our shooting parameter t.

References

Baker, D.A., 2000. Long-distance vascular transport of endogenous hormones in plants and their role in source:sink regulation. Isr. J. Plant Sci. 48 (3), 199–203.

Band, L.R., Wells, D.M., Larrieu, A., Sun, J., Middleton, A.M., French, A.P., Brunoud, G., Sato, E.M., Wilson, M.H., Péret, B., Oliva, M., andSairanen, I.Swarup.Ranjan., Parry, G., Ljung, K., Beeckman, T., Garibaldi, J.M., Estelle, M., Owen, M.R., Vissenberg, K., Hodgman, T.C., Pridmore, T.P., King, J.R., Vernoux, T., Bennett, M.J., 2012. Root gravitropism is regulated by a transient lateral auxin gradient controlled by a tipping-point mechanism. Proc. Natl. Acad. Sci. 109 (12), 4668–4673.

van den Berg, T., Korver, R.A., Testerink, C., ten Tusscher, K.H., 2016. Modeling halotropism: a key role for root tip architecture and reflux loop remodeling in redistributing auxin. Development 143 (18), 3350–3362.

Bhalerao, R.P., Eklöf, J., Ljung, K., Marchant, A., Bennett, M., Sandberg, G., 2002. Shoot-derived auxin is essential for early lateral root emergence in *arabidopsis seedlings*. Plant J. 29 (3), 325–332.

Bidel, L., Pages, L., Riviere, L., Pelloux, G., Lorendeau, J., 2000. MassFlowDyn I: a carbon transport and partitioning model for root system architecture. Ann. Botany 85 (6), 869–886.

Bishopp, A., Lehesranta, S., Vatén, A., Help, H., El-Showk, S., Scheres, B., Helariutta, K., Mähönen, A.P., Sakakibara, H., Helariutta, Y., 2011. Phloem-transported cytokinin regulates polar auxin transport and maintains vascular pattern in the root meristem. Curr. Biol. 21 (11), 927–932.

Bret-Harte, M.S., Silk, W.K., 1994. Nonvascular, symplasmic diffusion of sucrose cannot satisfy the carbon demands of growth in the primary root tip of *Zea mays* L. Plant Physiol. 105 (1), 19–33.

Brunkard, J.O., Zambryski, P., 2019. Plant cell–cell transport via plasmodesmata is regulated by light and the circadian clock. Plant Physiol. 181 (4), 1459–1467.

ChemSpider, Royal Society of Chemistry, 2021a. CSID:391354 – brassinolide. http://www.chemspider.com/Chemical-Structure.391354.html. (Accessed: 2021-09-17).

ChemSpider, Royal Society of Chemistry, 2021b. CSID:395716 – trans-zeatin. http://www.chemspider.com/Chemical-Structure.395716.html. (Accessed: 2021-09-17).

ChemSpider, Royal Society of Chemistry, 2021c. CSID:6223 – giberellic acid. http://www.chemspider.com/Chemical-Structure.6223.html. (Accessed: 2021-09-17).

Chhun, T., Uno, Y., Taketa, S., Azuma, T., Ichii, M., Okamoto, T., Tsurumi, S., 2007. Saturated humidity accelerates lateral root development in rice (*Oryza sativa* L.) seedlings by increasing phloem-based auxin transport. J. Exp. Bot. 58 (7), 1695–1704.

De Rybel, B., Mähönen, A.P., Helariutta, Y., Weijers, D., 2016. Plant vascular development: from early specification to differentiation. Nature Rev. Mol. Cell Biol. 17 (1), 30–40.

Gong, X., Liu, M., Zhang, L., Ruan, Y., Ding, R., Ji, Y., Zhang, N., Zhang, S., Farmer, J., Wang, C., 2015. Arabidopsis atsuc2 and atsuc4, encoding sucrose transporters, are required for abiotic stress tolerance in an aba-dependent pathway. Physiol. Plant. 153 (1), 119–136.

Gosting, L.J., Morris, M.S., 1949. Diffusion studies on dilute aqueous sucrose solutions at 1 and 25° with the Gouy interference method. J. Am. Chem. Soc. 71 (6), 1998–2006.

Grieneisen, V.A., Xu, J., Marée, A.F., Hogeweg, P., Scheres, B., 2007. Auxin transport is sufficient to generate a maximum and gradient guiding root growth. Nature 449, 1008–1013.

van den Herik, B., Bergonzi, S., Bachem, C.W., Ten Tusscher, K., 2021. Modelling the physiological relevance of sucrose export repression by an flowering time homolog in the long-distance phloem of potato. Plant Cell Environ. 44 (3), 792–806.

Imlau, A., Truernit, E., Sauer, N., 1999. Cell-to-cell and long-distance trafficking of the green fluorescent protein in the phloem and symplastic unloading of the protein into sink tissues. Plant Cell 11 (3), 309–322.

Jensen, K.H., Berg-Sørensen, K., Bruus, H., Holbrook, N.M., Liesche, J., Schulz, A., Zwieniecki, M.A., Bohr, T., 2016. Sap flow and sugar transport in plants. Rev. Modern Phys. 88 (3), 035007.

Jensen, K.H., Berg-Sørensen, K., Friis, S.M., Bohr, T., 2012. Analytic solutions and universal properties of sugar loading models in Münch phloem flow. J. Theoret. Biol. 304, 286–296.

Jensen, K.H., Lee, J., Bohr, T., Bruus, H., Holbrook, N.M., Zwieniecki, M., 2011. Optimality of the Münch mechanism for translocation of sugars in plants. J. R. Soc. Interface 8 (61), 1155–1165.

Jensen, K.H., Rio, E., Hansen, R., Clanet, C., Bohr, T., 2009. Osmotically driven pipe flows and their relation to sugar transport in plants. J. Fluid Mech. 636, 371–396.

Jensen, K.H., Savage, J.A., Holbrook, N.M., 2013. Optimal concentration for sugar transport in plants. J. R. Soc. Interface 10 (83), 20130055.

Kedem, O., Katchalsky, A., 1958. Thermodynamic analysis of the permeability of biological membranes to non-electrolytes. Biochim. Biophys. Acta 27, 229–246.
Kiba, T., Kudo, T., Kojima, M., Sakakibara, H., 2011. Hormonal control of nitrogen acquisition: roles of auxin, abscisic acid, and cytokinin. J. Exp. Bot. 62 (4), 1399–1409.
Knox, K., Paterlini, A., Thomson, S., Oparka, K., 2018. The coumarin glucoside, esculin, reveals rapid changes in phloem-transport velocity in response to environmental cues. Plant Physiol. 178 (2), 795–807.
Kramer, M., Went, F., 1949. The nature of the auxin in tomato stem tips. Plant Physiol. 24 (2), 207.
Lacombe, B., Achard, P., 2016. Long-distance transport of phytohormones through the plant vascular system. Curr. Opini. Plant Biol. 34, 1–8.
Martin, T., Oswald, O., Graham, I.A., 2002. Arabidopsis seedling growth, storage lipid mobilization, and photosynthetic gene expression are regulated by carbon: nitrogen availability. Plant Physiol. 128 (2), 472–481.
Mellor, N.L., Voß, U., Janes, G., Bennett, M.J., Wells, D.M., Band, L.R., 2020. Auxin fluxes through plasmodesmata modify root-tip auxin distribution. Development 147 (6).
Minchin, P., Thorpe, M., Farrar, J., 1993. A simple mechanistic model of phloem transport which explains sink priority. J. Exp. Bot. 44 (5), 947–955.
Münch, E., 1926. Dynamik der saftstromungen. Ber. Deut. Bot. Ges. 44, 68–71.
Nakad, M., Witelski, T., Domec, J.-C., Sevanto, S., Katul, G., 2021. Taylor dispersion in osmotically driven laminar flows in phloem. J. Fluid Mech. 913.
Oparka, K., Duckett, C., Prior, D., Fisher, D., 1994. Real-time imaging of phloem unloading in the root tip of *Arabidopsis*. Plant J. 6 (5), 759–766.
Payvandi, S., Daly, K.R., Zygalakis, K., Roose, T., 2014. Mathematical modelling of the phloem: The importance of diffusion on sugar transport at osmotic equilibrium. Bull. Math. Biol. 76 (11), 2834–2865.
Regnault, T., Davière, J.-M., Wild, M., Sakvarelidze-Achard, L., Heintz, D., Bergua, E.C., Diaz, I.L., Gong, F., Hedden, P., Achard, P., 2015. The gibberellin precursor GA_{12} acts as a long-distance growth signal in Arabidopsis. Nature Plants 1 (6), 15073.
Ross-Elliott, T.J., Jensen, K.H., Haaning, K.S., Wager, B.M., Knoblauch, J., Howell, A.H., Mullendore, D.L., Monteith, A.G., Paultre, D., Yan, D., Otero, S., Bourdon, M., Sager, R., Lee, J.-Y., Helariutta, Y., Knoblauch, M., Oparka, K., 2017. Phloem unloading in arabidopsis roots is convective and regulated by the phloem-pole pericycle. Elife 6, e24125.
Sager, R., Lee, J.-Y., 2014. Plasmodesmata in integrated cell signalling: insights from development and environmental signals and stresses. J. Exp. Bot. 65 (22), 6337–6358.
Sasaki, T., Suzaki, T., Soyano, T., Kojima, M., Sakakibara, H., Kawaguchi, M., 2014. Shoot-derived cytokinins systemically regulate root nodulation. Nature Commun. 5 (1), 1–9.
Staverman, A., 1951. The theory of measurement of osmotic pressure. Recueil Des Travaux Chimiques Des Pays-Bas 70 (4), 344–352.
Taiz, L., Zeiger, E., 2010. Plant Physiology, fifth ed. Sinauer Associates Inc.
Tamas, I.A., Davies, P.J., 2016. Dynamics and control of phloem loading of indole-3-acetic acid in seedling cotyledons of *Ricinus communis*. J. Exp. Bot. 67 (15), 4755–4765.
Thompson, M.V., Holbrook, N.M., 2003a. Application of a single-solute non-steady-state phloem model to the study of long-distance assimilate transport. J. Theoret. Biol. 220 (4), 419–455.
Thompson, M.V., Holbrook, N.M., 2003b. Scaling phloem transport: water potential equilibrium and osmoregulatory flow. Plant Cell Environ. 26 (9), 1561–1577.
Truskey, G.A., Yuan, F., Katz, D.F., 2010a. Chapter 4: Approximate Methods for the Analysis of Complex Physiological Flow. 19, Pearson, pp. 6–240.
Truskey, G.A., Yuan, F., Katz, D.F., 2010b. Chapter 9: Transvascular Transport. 46, Pearson, pp. 5–485.
Xu, Q., Chen, S., Yunjuan, R., Chen, S., Liesche, J., 2018. Regulation of sucrose transporters and phloem loading in response to environmental cues. Plant Physiol. 176 (1), 930–945.
Zhang, Y., Kilambi, H.V., Liu, J., Bar, H., Lazary, S., Egbaria, A., Ripper, D., Charrier, L., Belew, Z.M., Wulff, N., et al., 2021. Aba homeostasis and long-distance translocation are redundantly regulated by abcg aba importers. Sci. Adv. 7 (43), eabf6069.